

Supporting information

**Switching Intramolecular Singlet Fission in Tetracene Dimer *via*
Subtle Change in Bridge**

T. Wang, S. Zhang, Y.-T. Ding, B.-Y. Zhang, B.Y. Yu, R. Xu, Z.-X. Liu, C.-L. Sun,
C.F. Zhang, Q. Wang and H.-L. Zhang

^aState Key Laboratory of Applied Organic Chemistry (SKLAOC), Key Laboratory of
Special Function Materials and Structure Design (MOE), College of Chemistry and
Chemical Engineering, Lanzhou University, Lanzhou, 730000, China. E-mail: haoli.
zhang@lzu.edu.cn

^bNational Laboratory of Solid State Microstructures, Collaborative Innovation Centre
of Advanced Microstructures, School of Physics, Nanjing University, Nanjing,
210093, China. E-mail: cfzhang@nju.edu.cn

Table of Contents

1. Materials and Methods	3
2. Experimental section.....	6
Steady-state spectra	6
Transient absorption spectroscopy.....	10
Triplet sensitization.....	19
Quantum chemical calculation.....	21
Synthetic information	30
^1H and ^{13}C NMR spectra	33
Cartesian coordinates	39
3. Reference.....	46

1. Materials and Methods

All the reagents and solvents were used as received. Chemicals were purchased from commercial suppliers: TCI America, Alfa Aesar and Innochem. ^1H NMR spectra were measured in CDCl_3 on 400MHz Liquid State NMR Spectrometer (AVANCE III 400). The high resolution mass spectra (HRMS) were obtained using Bruker microTOF-Q20453.

Steady-state and time-resolved fluorescence spectroscopy characterization

The steady-state absorption spectrum was obtained by a T6 UV-Vis spectrometer (Purkinje General, China). The absolute photoluminescence quantum yields (PLQY) of the molecules were measured by an FLS920 fluorescence spectrometer using an integrating sphere (Edinburgh, UK). The steady-state and time-resolved emission spectra were acquired on a spectrometer equipped with a liquid-nitrogen-cooled silicon charge-coupled device (CCD) (400BR_eXcelon, PyLoN, Princeton Instruments) and a 515 nm laser (PHAROS). The fluorescence decay profiles were recorded by the technique of time-correlated single-photon counting (Swabian instruments).

Femtosecond and nanosecond transient absorption spectroscopy (fs- and ns-TA)

Pulses of about 100 fs duration at a repetition rate of 1 kHz and a wavelength centred at 800 nm was generated by a Coherent Chameleon oscillator seeded a Ti/sapphire regenerative amplifier (Coherent Legend Elite). A Light Conversion OPerA-Solo optical parametric amplifier (285-2600 nm) produces the 550 nm pump pulse. The pump fluence was kept in the linear regime. By focusing a small portion of

800 nm beam on the sapphire plate, a white probe pulse was obtained. The chirp of the supercontinuum probe was corrected with an error within 100 fs over the entire spectral range. The TA signal was then analyzed by a silicon CCD (S11071, Hamamatsu) mounted on a monochromator (Acton 2358, Princeton Instrument) at 1 kHz enabled by a custom-built control board from Entwicklungsbuero Stresing. The signal-to-noise ratio in differential transmission was better than 10^{-4} . All the spectroscopic measurements were carried out at room temperature. For nanosecond TA spectroscopy, we replaced the femtosecond pump beam with a frequency-doubled sub-nanosecond laser (Piccolo AOT MOPA, InnoLas) at 532 nm (pulse duration, ~ 0.8 ns). The probe beams were generated by focusing a small portion of the femtosecond laser beam onto a 3 mm thick sapphire plate. The laser was synchronized to the probe pulse with a desired delay by an electronic delay generator (SRS DG645, Stanford Research System). The data recording procedure were the same as used for fs-TA spectroscopy. The stability of the samples was spectrophotometrically checked before and after each experiment.

Global and Target Analysis (GTA)

Singular value decomposition (SVD) was performed to get preliminary estimation of the species involved. Based on the results of SVD, target (differential equation-based) analysis is accomplished using the Glotaran software package.¹⁻³ The parameters given by the previous model were returned to get optimized results, judged by the residual matrix. The transient absorption data were modelled using the following scheme.

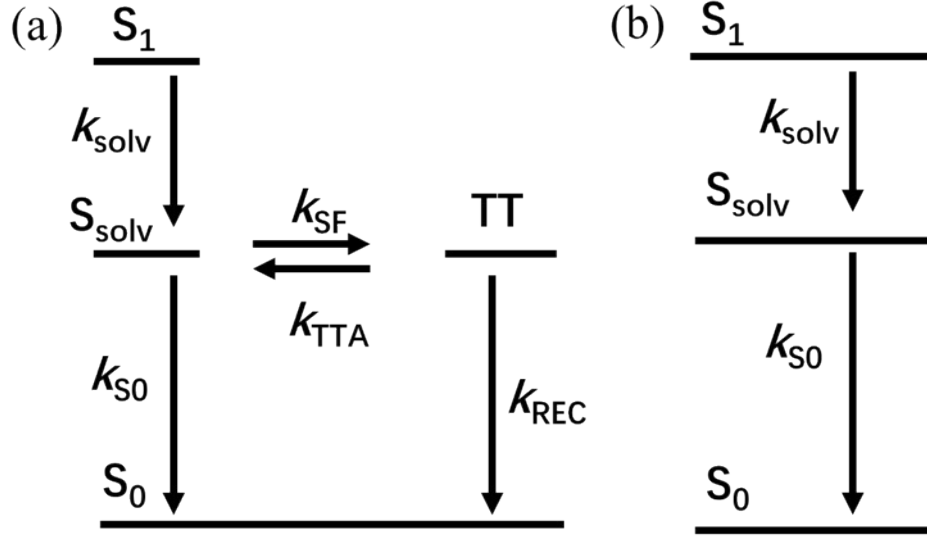


Figure S1. A model for target analysis of 2T-DPP (a) and 2T-DOP (b) for fs-TA data. For 2T-DOP in dichloromethane (DCM), S_{solv} is replaced by S_{solv}' .

In Fig. S1a, the population of S_1 , S_{solv} and TT can be described using the following kinetic equations.

$$\frac{d[S_1]}{dt} = -k_{solv}[S_1] \quad (S1)$$

$$\frac{d[S_{solv}]}{dt} = k_{solv}[S_1] + k_{TTA}[TT] - (k_{S0} + k_{SF})[S_{solv}] \quad (S2)$$

$$\frac{d[TT]}{dt} = k_{SF}[S_{solv}] - (k_{TTA} + k_{REC})[TT] \quad (S3)$$

In Fig. S1b, the population of S_1 and S_{solv} can be described using the following kinetic equations.

$$\frac{d[S_1]}{dt} = -k_{solv}[S_1] \quad (S4)$$

$$\frac{d[S_{solv}]}{dt} = k_{solv}[S_1] - k_{S0}[S_{solv}] \quad (S5)$$

2. Experimental section

Steady-state spectra

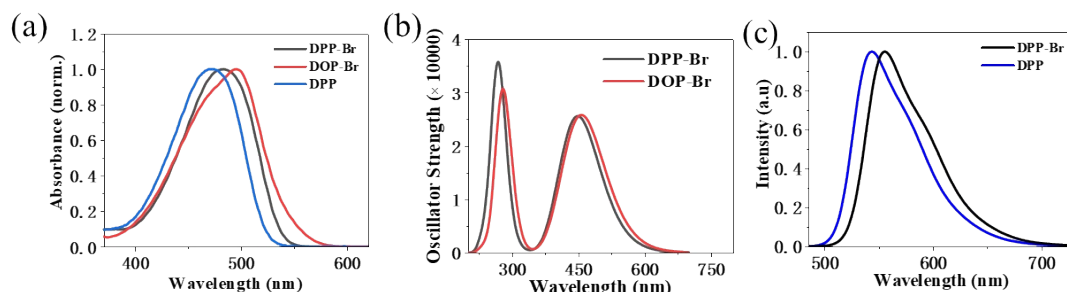


Figure S2. (a) Absorption spectra of DPP-Br (Compound 2, black), DOP-Br (Compound 3, red) and DPP (blue) in DCM. We have tried to synthesized *N,O*-alkylation product (DOP). However, the alkylation of DPP core without bromine atoms on both sides only leads to *O,O*-alkylation and *N,N*-alkylation products. Instead, the DPP and DPP-Br are obtained. (b) Calculated electronic absorption spectra of DPP-Br and DOP-Br in DCM. (c) Fluorescence spectra of DPP-Br and DPP in DCM. The fluorescence spectrum of DOP-Br was not obtained due to the extremely low fluorescence quantum yield.

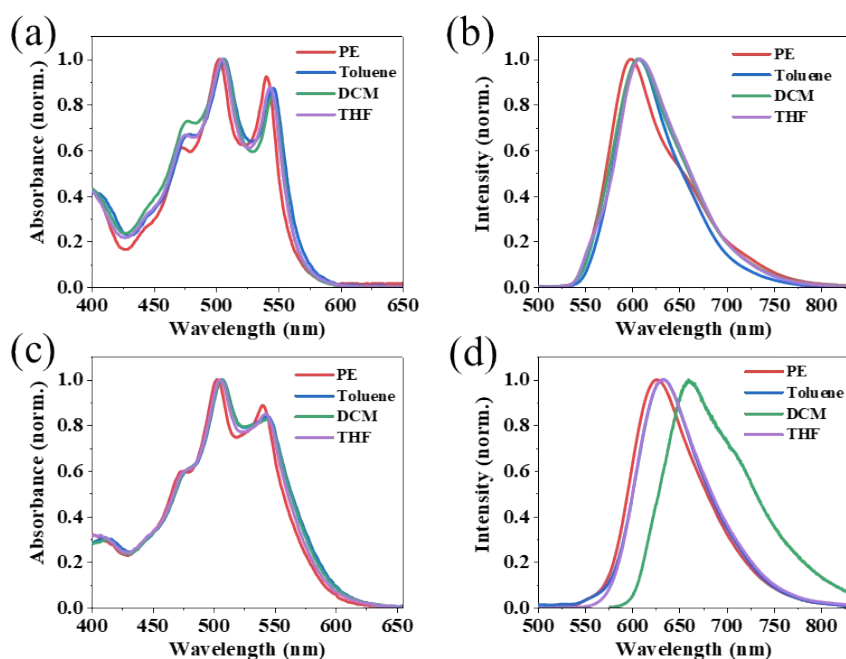


Figure S3. Normalized steady-state absorption spectra and emission spectra of 2T-DPP (a, b), 2T-DOP (c, d) in petroleum ether (PE), toluene, DCM and tetrahydrofuran (THF).

Table S1. Solvent polarity⁴ and solvent-dependent steady-state optical parameters of 2T-DPP and 2T-DOP.

		PE	Toluene	DCM	THF
	polarity	0.01	2.4	3.4	4.0
DPP	λ_{0-0} (nm) ^a	-	-	472	-
	λ_{em} (nm) ^b	-	-	547	-
	Stokes shift (nm)	-	-	75	-
2T-DPP	λ_{0-0} (nm) ^a	540	546	545	544
	λ_{em} (nm) ^b	600	607	606	608
	Stokes shift (nm)	60	61	61	65
2T-DOP	λ_{0-0} (nm) ^a	540	543	543	544
	λ_{em} (nm) ^b	629	633	659	633
	Stokes shift (nm)	89	90	116	89

^a λ_{0-0} is the wavelength of 0-0 absorption peak. ^b λ_{em} is the maximum emission wavelength.

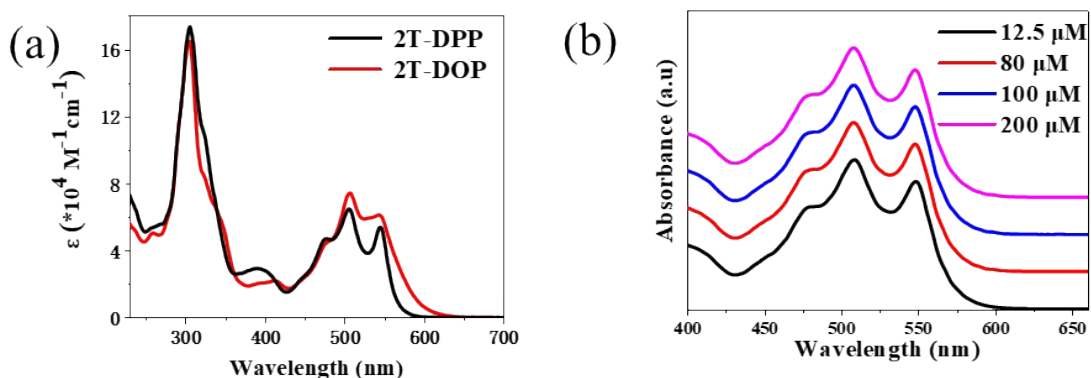


Figure S4. (a) The absorption spectra of 2T-DPP (black) and 2T-DOP (red) including short wavelength. (b) Normalized absorption spectra of 2T-DPP in DCM from 12.5 μ M to 200 μ M.

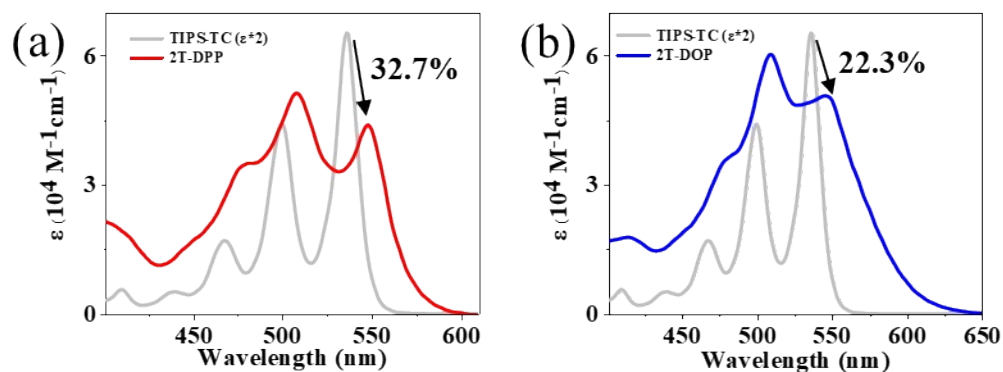


Figure S5. Electronic absorption spectra of 2T-DPP (a) and 2T-DOP (b) compared with TIPS-TC. The extinction coefficient of TIPS-TC was multiplied by 2 for clarity.

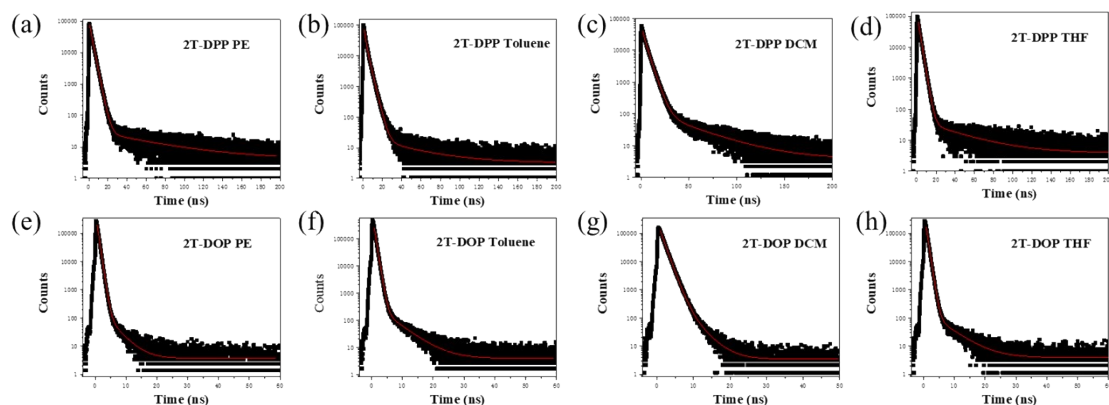


Figure S6. Fluorescence decay profiles of 2T-DPP (a, b, c and d) and 2T-DOP (e, f, g and h). The obtained lifetimes are summarized in Table S2. The excitation wavelength was 515 nm. The solid lines are fitting curves by the tri-exponential decay for 2T-DPP and double-exponential decay for 2T-DOP.

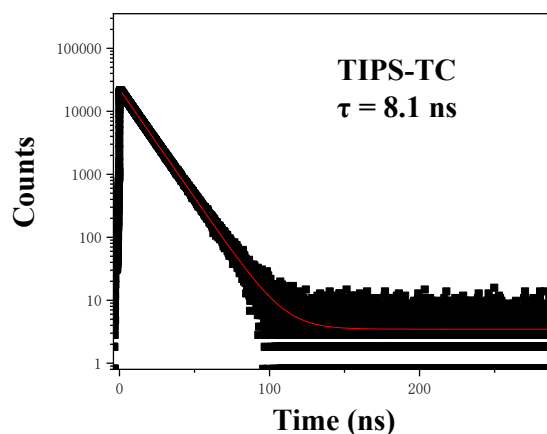


Figure S7. Fluorescence decay profiles of TIPS-TC.

Table S2. Lifetime of singlet state in 2T-DPP, 2T-DOP and TIPS-TC.

Compound	Solvent	τ_1 (ns) ^b	τ_2 (ns) ^a	τ_3 (ns) ^a	τ_1 (ps)	τ_{TTA} (ps) ^b
2T-DPP	PE	< 0.1 (52.8 %)	2.8 (47.2 %)	13.9 (< 0.1 %)	5.5 ^b	58.8
	Toluene	< 0.1 (49.1 %)	2.9 (50.0 %)	10.2 (0.9 %)	4.1 ^b	66.7
	DCM	< 0.1 (35.1 %)	4.7 (64.7 %)	10.7 (0.2 %)	4.0 ^b	55.6
	THF	< 0.1 (37.6 %)	2.3 (62.4 %)	12.2 (< 0.1 %)	3.8 ^b	58.9
2T-DOP	PE	0.6 (99.9 %)	3.5 (0.1 %)	-	556 ^c	-
	Toluene	0.6 (99.5 %)	5.1 (0.5 %)	-	556 ^c	-
	DCM	1.2 (99.3 %)	3.3 (0.7 %)	-	1250 ^c	-
	THF	0.6 (99.9 %)	5.4 (0.1 %)	-	588 ^c	-
TIPS-TC	DCM	8.1 (100 %)	-	-	-	-

^aCalculated by using fluorescence decay profiles. ^bCalculated by using fs-TA for 2T-DPP, $\tau_1 = 1/k_{\text{solv}} + 1/k_{\text{SF}}$ and $\tau_{\text{TTA}} = 1/k_{\text{TTA}}$. ^cCalculated by using fs-TA for 2T-DOP, $\tau_1 = 1/k_{\text{solv}} + 1/k_{\text{S0}}$.

Herein, the fluorescence decay profiles and corresponding lifetimes of 2T-DPP and 2T-DOP are shown in Fig. S6 and Table S2. The lifetimes were fitted by the tri-exponential decay for 2T-DPP. However, the short-lived component (τ_1) is below the resolution limit of the instrument, so that is meaningless. Therefore, the values of τ_1 were calculated by using fs-TA data.⁵ The lifetimes of singlet state derived from fluorescence decay profiles and fs-TA data have been both provided in Table S2. For instance, in PE, the fluorescence decay profile of 2T-DPP was fitted by the tri-

exponential decay, showing the presence of a long-lived fluorescent species ($\tau_3 = 13.9$ ns). It can be seen that 2T-DPP had long-lived fluorescent species in all solvents compared with monomer TIPS-TC ($\tau = 8.1$ ns), indicating the reverse process from TT to S_1 . In contrast, 2T-DOP did not show long-lived fluorescent specie.

Transient absorption spectroscopy

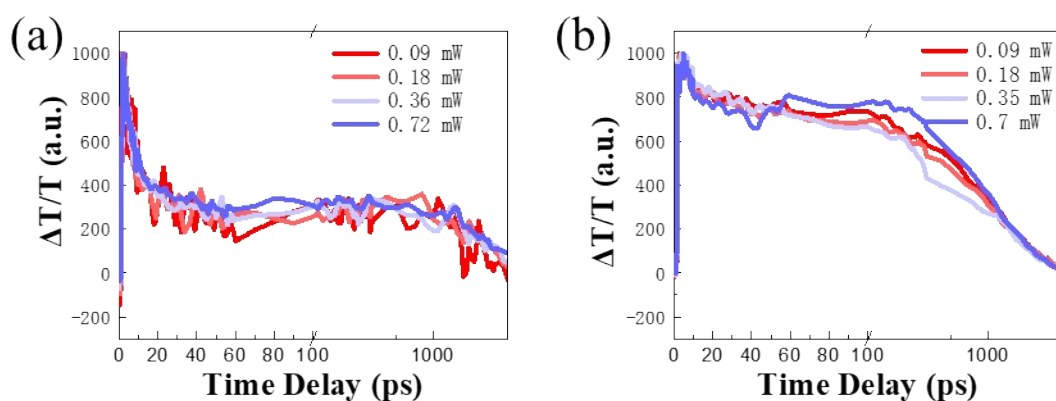


Figure S8. Pump power controlled fs-TA of 2T-DPP (a) and 2T-DOP (b) in toluene. Comparison of kinetics at 506 nm using different pump power. The kinetics scale linearly with pump power, and the kinetics are not varied. All the experiments are within the linear regime.

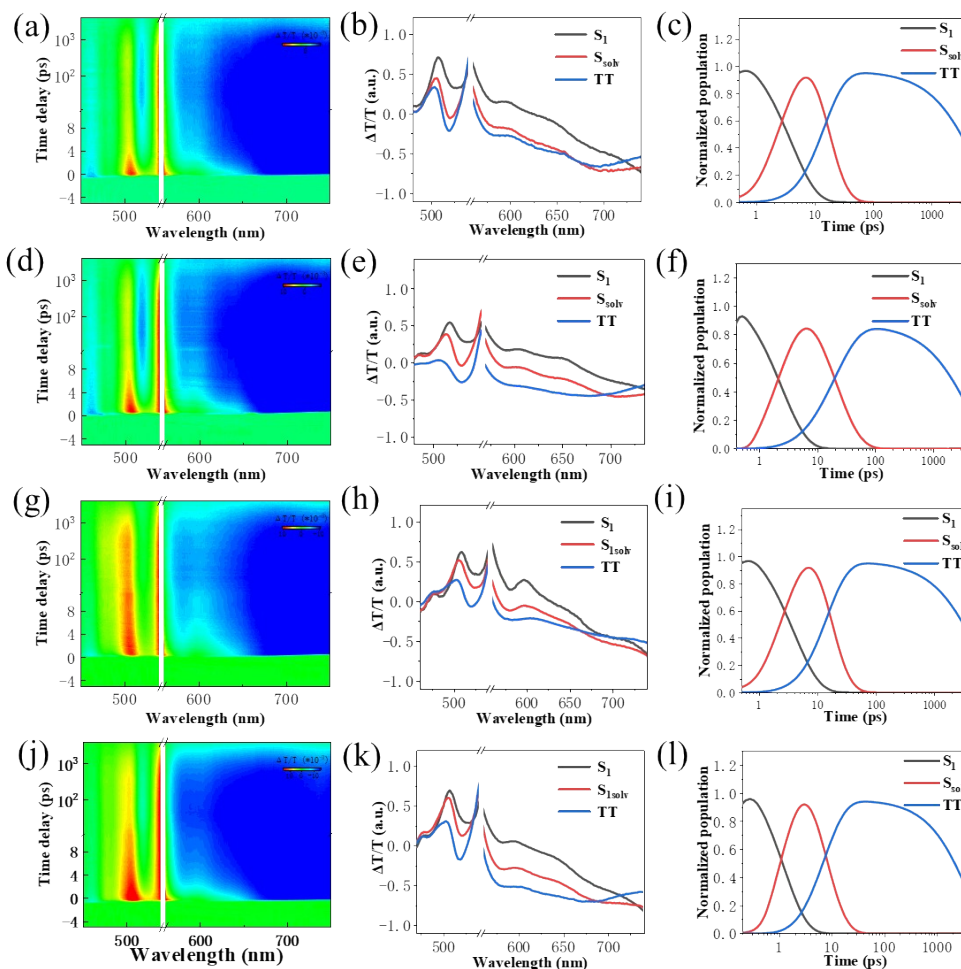


Figure S9. Transient absorption spectra of 2T-DPP in PE (a), toluene (d), DCM (g) and THF (j) excited at 550 nm (2 mW). The evolution-associated spectra (b, e, h and k) and respective population dynamics (c, f, i and l) from global fitting. The signal at 560 nm is quenched within 5 ps, then turns negative during SF, due to overlap between SE signal of S_1 state and negative signal of TT state. As shown in Fig. 3b and 4b, the TT species obtained from global analysis is in good agreement with the shape of the TA spectrum at 4 ns.

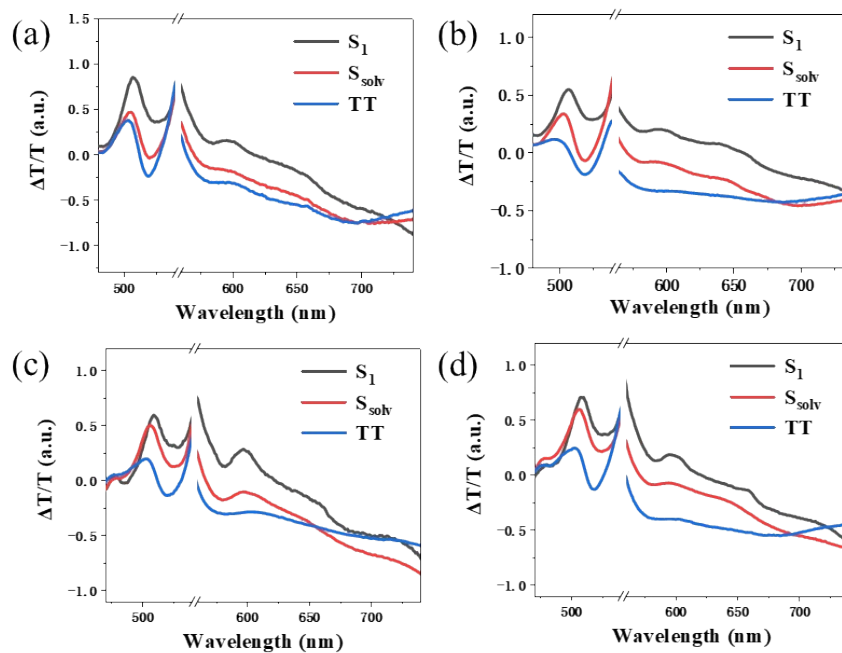


Figure S10. The species-associated spectra (SAS) of 2T-DPP from target analysis in PE (a), toluene (b), DCM (c) and THF (d). In Fig. S12 and S16, fitting curves match the raw data well, suggesting the accuracy of fitting.

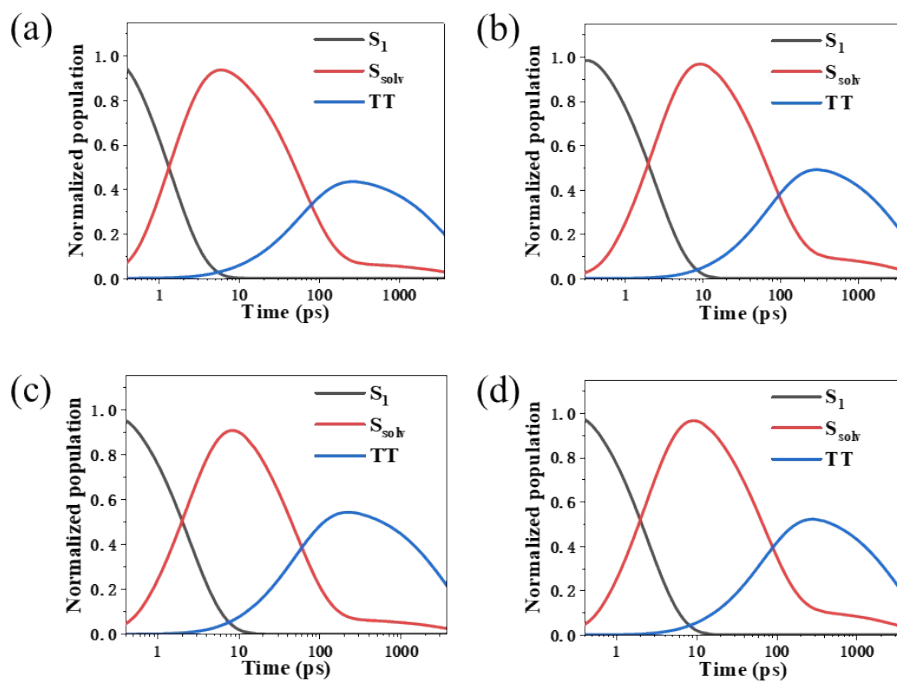


Figure S11. Respective population dynamics of 2T-DPP in DCM (a), toluene (b), DCM (c) and THF (d) from target analysis.

The global analysis and target analysis are the fits of data with a sequential model

and a compartmental model, respectively. The population obtained from target analysis refers to the real concentrations of the species. While, the total population of different species obtained from global analysis does not change before the last state returns to the ground state. Fig. 3 in the main text shows the target analysis data of 2T-DPP in toluene, which exhibits the information about real concentration change. The S_{solv} and TT states are in equilibrium when TT states decay to ground state, due to the backward reaction of TT state. The ratio of equilibrium constant between S_{solv} and TT state is calculated by $k_{\text{TTA}}:k_{\text{SF}}$. As an example, the relative ratio between S_{solv} and TT populations of 2T-DPP is about 1:5 with the decay of TT states in toluene.

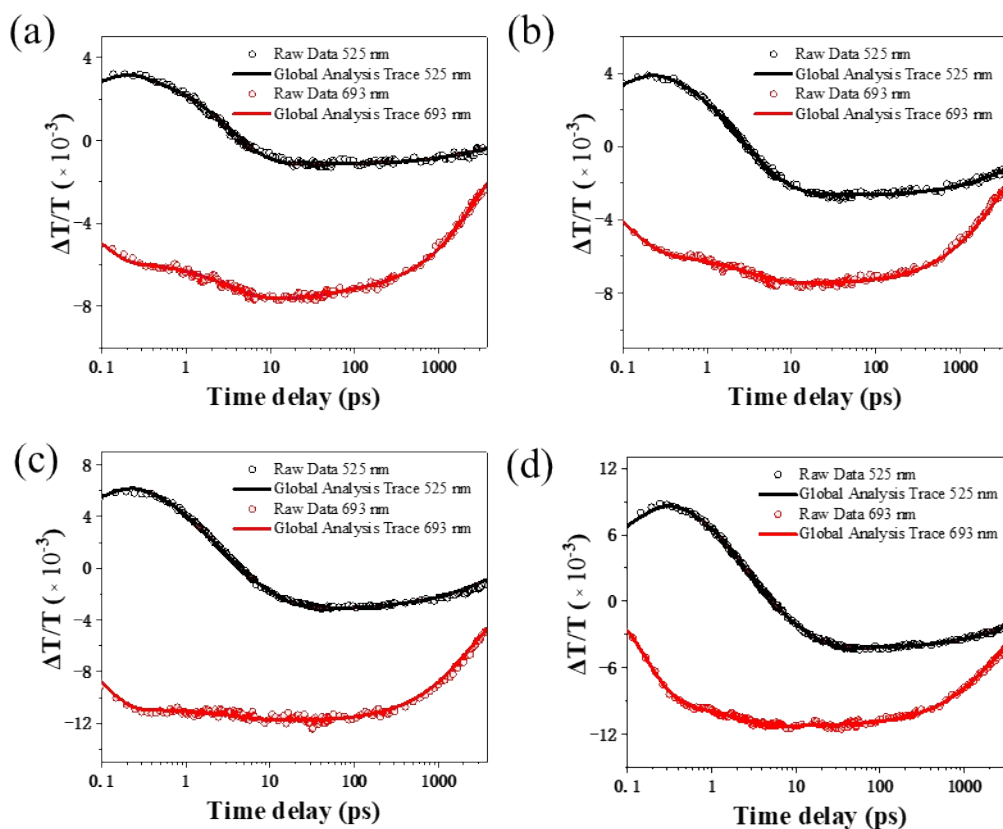


Figure S12. Comparison of kinetic cuts through the raw transient absorption data to the fits derived from a nonsequential decay model for 2T-DPP in PE (a), toluene (b), DCM (c) and THF (d).

Table S3. Rate constant for 2T-DPP by target analysis of fs-TA using the Glotaran program.

Compound	Parameters	PE	Toluene	DCM	THF
2T-DPP	$k_{S0} (10^7 \text{ s}^{-1})^a$	8.1 ± 0.1	8.1 ± 0.1	8.1 ± 0.1	8.1 ± 0.1
	$k_{TTA} (10^{10} \text{ s}^{-1})^b$	1.7 ± 0.1	1.5 ± 0.1	1.8 ± 0.1	1.7 ± 0.1
	$k_{REC} (10^8 \text{ s}^{-1})^b$	5.2 ± 0.1	3.4 ± 0.1	6.7 ± 0.2	1.5 ± 0.1

^aCalculated by using fluorescence lifetime of TIPS-TC. ^bCalculated by using the fs-TA.

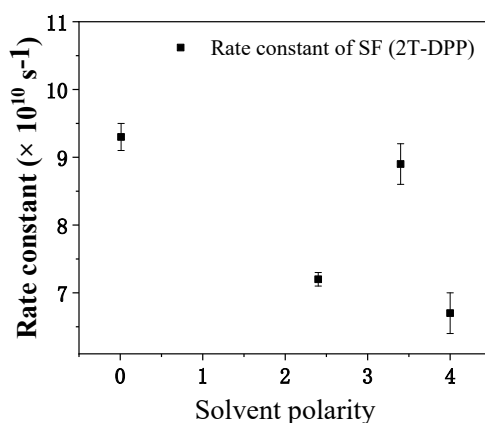


Figure S13. Solvent-dependent SF rate constants for 2T-DPP.

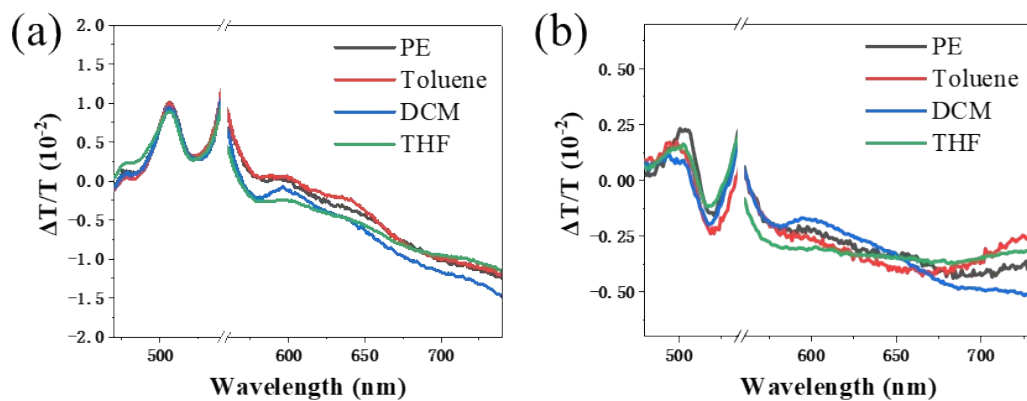


Figure S14. Transient spectra of singlet state at 1 ps (a) and triplet state 4000 ps (b) of 2T-DPP in different solvents.

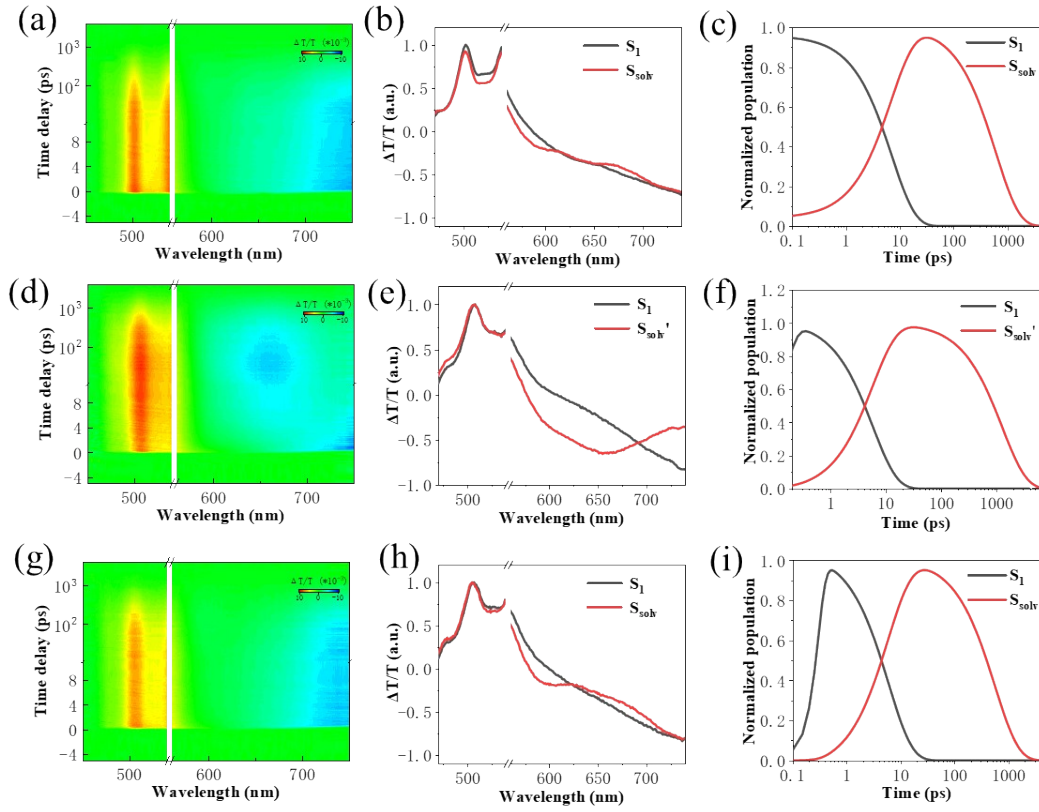


Figure S15. Transient absorption spectra of 2T-DOP in PE (a), DCM (d) and THF (g) excited at 550 nm (2 mW). The evolution-associated spectra (b, e and h) and respective population dynamics (c, f and i) from global fitting.

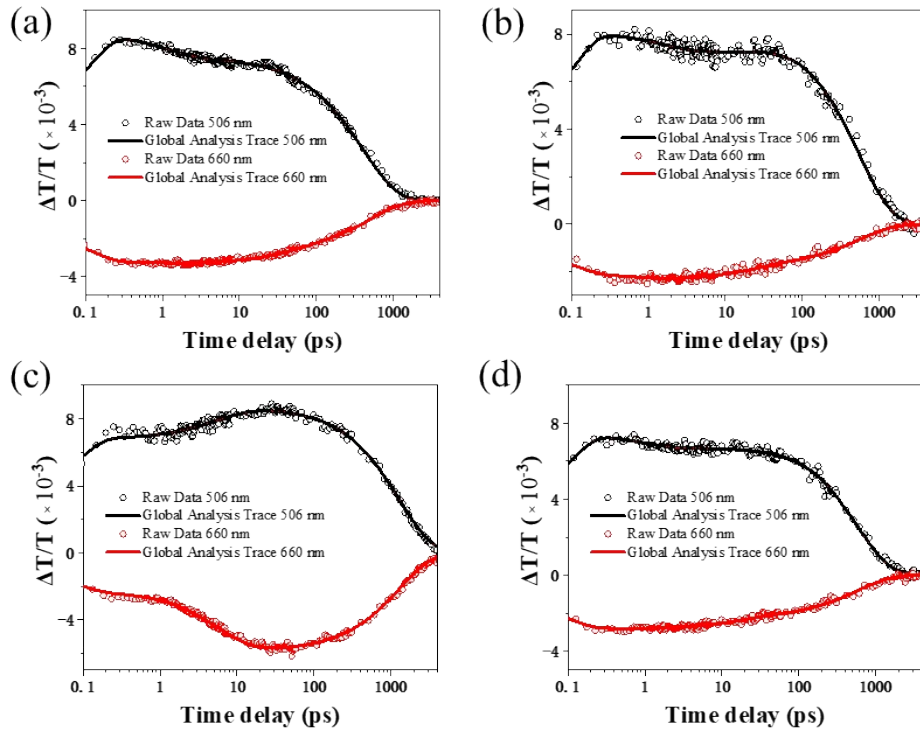


Figure S16. Comparison of kinetic cuts through the raw transient absorption data to the fits derived from a sequential decay model for 2T-DOP in PE (a), toluene (b), DCM (c) and THF (d).

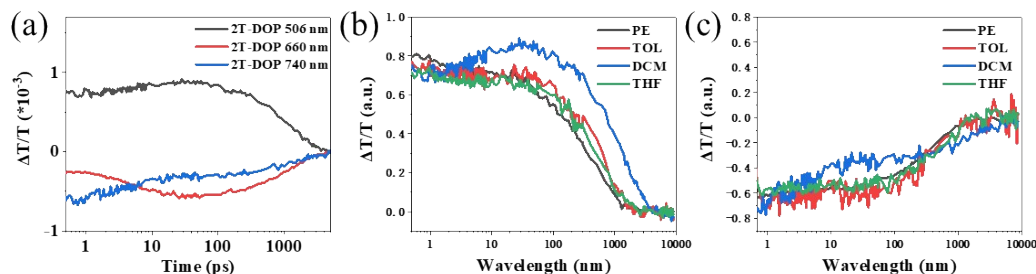


Figure S17. (a) The dynamic curves at 506 nm, 600 nm and 740 nm of 2T-DOP in DCM. Comparison of kinetics at 506 nm (b) and 650 nm (c) of 2T-DOP at different solvents.

As shown in Fig. S15e, 2T-DOP shows a distinct state featuring a negative peak around 660 nm at 100 ps in DCM, which is not the triplet state suggested by the sensitization experiment (Fig. S23). The PL spectrum of 2T-DOP in DCM ($\lambda_{\text{em}} = 659$ nm) shows an obvious red-shift compared to that in PE, toluene and THF ($\lambda_{\text{em}} \approx 630$ nm). The fitting to the fluorescence decay profiles suggests that the lifetime of this state ($\tau_1 = 1.2$ ns) is longer than that of S_{solv} state ($\tau_1 = 0.6$ ns) in other solvents. Based on above analysis, the second state of 2T-DOP in DCM is different and has been assigned as S_{solv}' state. The exact nature of the S_{solv}' state of 2T-DOP in DCM is unclear at the moment, which is beyond the scope of this work.

For 2T-DPP, the fs-TA and ns-TA spectra of the third state in DCM also shows slight difference with that in the other solvents. As shown in Fig. 3, S9 and S19, the spectra of the third state in PE, toluene and THF all show a peak around 690 nm. In contrast, the spectrum of the third state in DCM does not show this peak. However, as shown in Table 1 and S3, the lifetime of the third state in DCM is very similar to that

in other solvents, suggesting that the SF process is not altered in DCM. In the steady-state spectra, the emission spectrum in DCM is nearly the same, suggesting that the fluorescence based on TTA is similar. Based on the above analysis, though the third state in DCM exhibits slight spectral difference, the species can still be assigned as TT state.

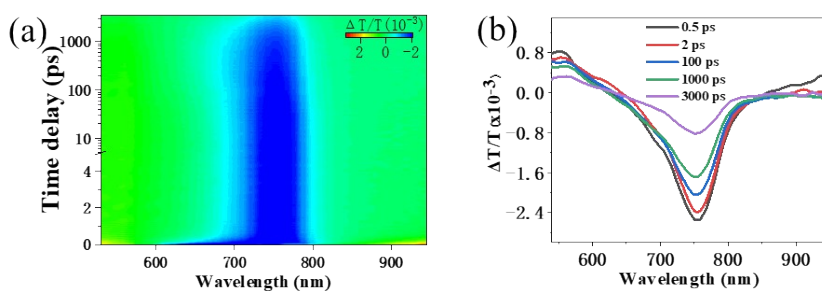


Figure S18. (a) Transient absorption spectra of DPP, excited at 510 nm (2 mW) in DCM. (b) fs-TA spectra at different delay times.

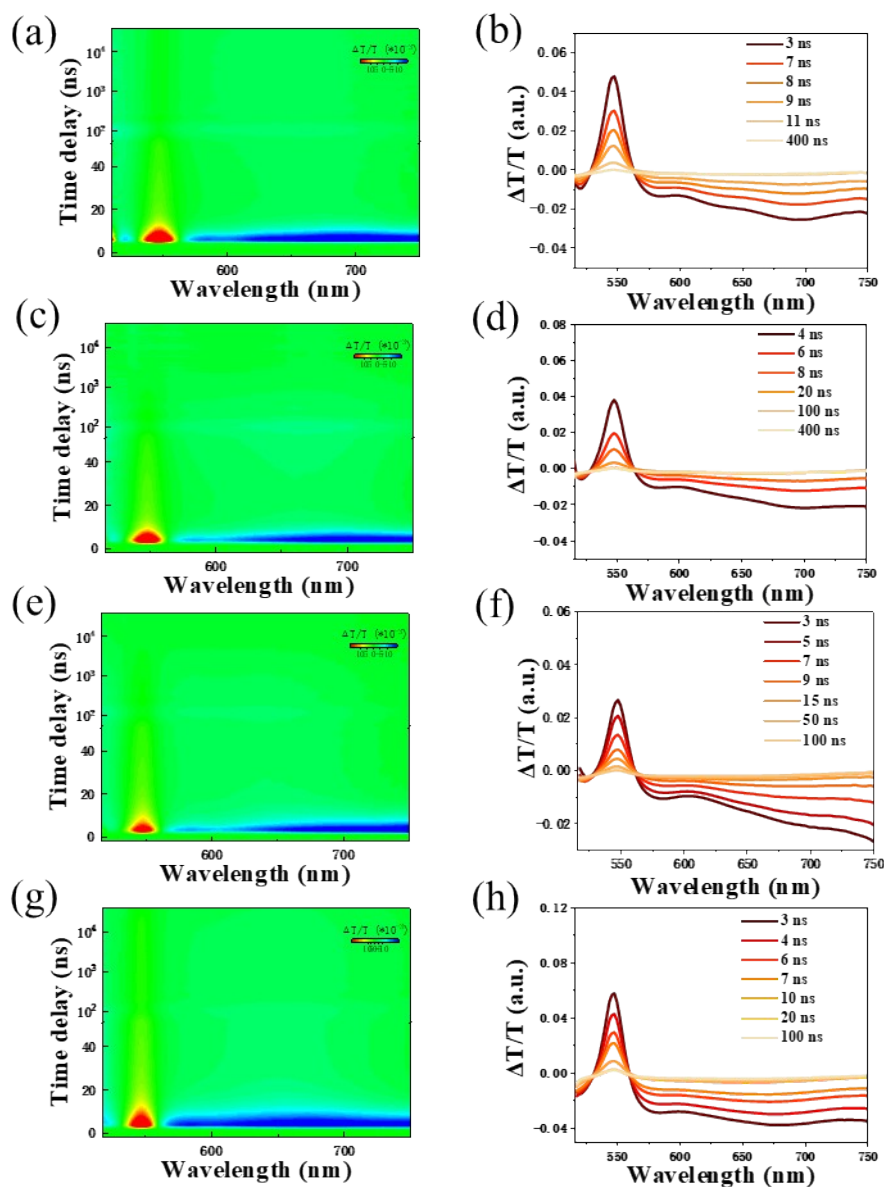


Figure S19. ns-TA spectra of 2T-DPP in PE (a), Toluene (c), DCM (e) and THF (g). Time-resolved spectra at different times of 2T-DPP in PE (b), Toluene (d), DCM (f) and THF (h).

The signals of 2T-DPP decay fast after 4 ns, indicating that the TT states are generated within the first 4 ns. Meanwhile, the triplet of 2T-DPP may transfer to DPP due to the similar energy level between TIPS-TC and DPP. However, it is difficult to perform global and target analysis due to the very weak signals of DPP' triplet state.

Triplet sensitization

The delta epsilon spectra for triplet states of TIPS-TC and DPP were determined by triplet sensitization experiments using a solution of PtOEP and TIPS-TC or DPP excited at 532 nm. Triplets of PtOEP generated by intersystem crossing are transferred to TIPS-TC and DPP.

The total number of photons per pump pulse (532 nm) are $1.07 \times 10^{12} \text{ pulse}^{-1}$ using the following expression.

$$\frac{\text{photons}}{\text{pulse}} = \frac{\text{power}}{(\text{per rate})(\text{energy per photon})} \quad (\text{S6})$$

The concentration of sensitized dimer was then calculated using the population from the expression above along with the pump spot size ($d = 245 \text{ } \mu\text{m}$) and cuvette length ($L = 0.1 \text{ cm}$) to calculate the volume based on the following equation.

$$V = \text{Area} * d = \pi \left(\frac{d}{2}\right)^2 * L \quad (\text{S7})$$

The intersystem crossing yield of PtOEP was 100 % and the triplet transfer efficiency (Φ_{Transfer}) was measured in relation to pure PtOEP (a lifetime of $16.32 \text{ } \mu\text{s}$ (τ) in degassed DCM). The following expression were used.

$$N_{\text{triplet}} = (1 - 10^{-\text{Abs.}}) \frac{E_{\text{pump}}}{E_{\text{photon}}} * 100 \% * \frac{1/\tau_{\text{sens}}}{1/\tau_{\text{sens}} + 1/\tau} \quad (\text{S8})$$

The delta epsilon spectra for TIPS-TC and DPP from the concentration and ΔAbs using the following expression.

$$\Delta\varepsilon = \frac{\Delta Abs.}{\left(\frac{N_{triplet}}{V}\right) * L} \quad (S9)$$

The calculated delta epsilon T₁ spectra for TIPS-TC and DPP are shown below.

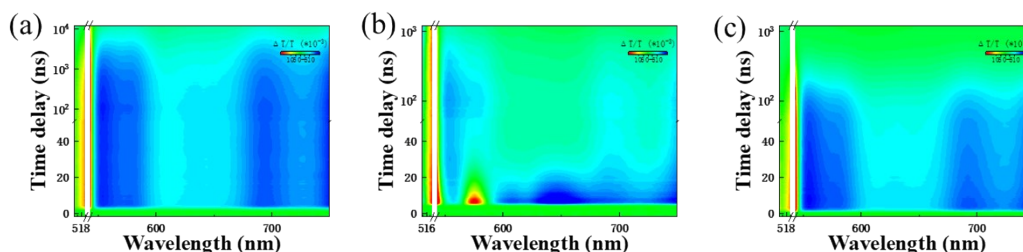


Figure S20. (a) Nanosecond transient absorption spectra of PtOEP. Sensitized nanosecond transient absorption spectra of TIPS-TC (b) and DPP (c).

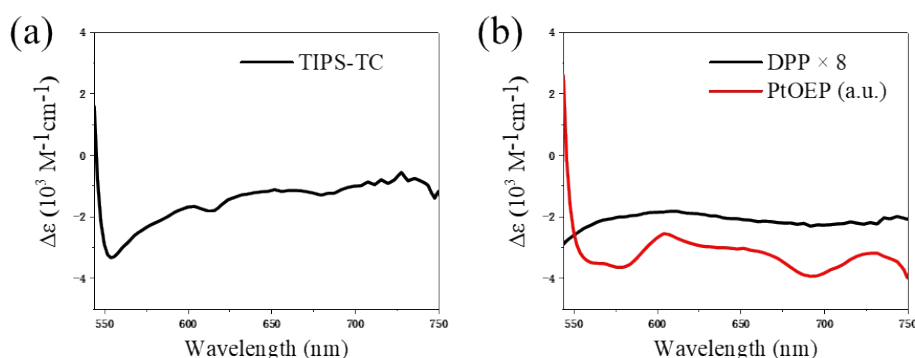


Figure S21. Delta epsilon spectra for triplet of TIPS-TC (a) and DPP (b). The triplet spectrum of DPP is multiplied by 8 for clarity and PtOEP's triplet is also shown. The TT yield of 2T-DPP cannot be obtained *via* the sensitization method because the triplet energy transfer efficient from PtOEP to 2T-DPP cannot be determined. The triplet yields were estimated using the state populations obtained from the nonsequential kinetic model by doubling the corresponding TT populations.

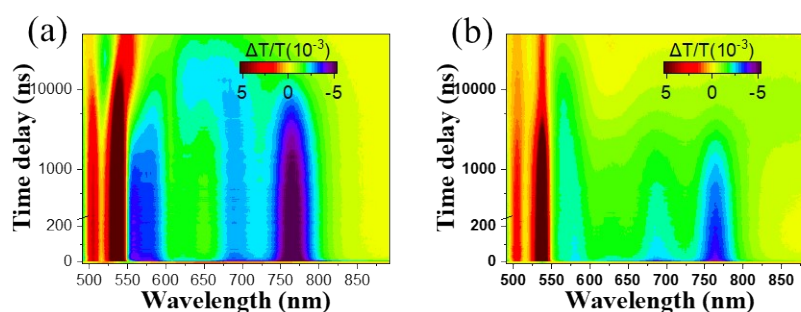


Figure S22. Sensitized nanosecond transient absorption spectra of 2T-DPP (a) and 2T-DOP (b).

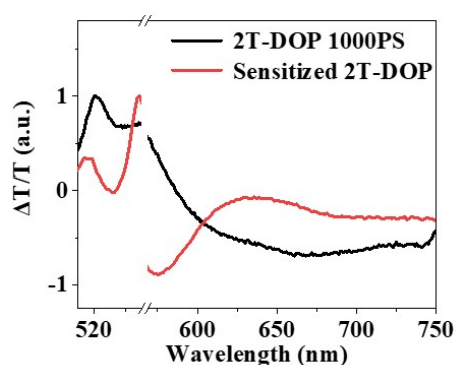


Figure S23. Comparison of the spectra obtained at 1000 ps (black) from fs-TA data and the sensitized triplet state (red) of 2T-DOP.

Quantum chemical calculation

The isopropyl groups of 2T-DPP and 2T-DOP were modeled by methyl groups to reduce computational cost. The geometries of DPP-Br, DOP-Br, 2T-DPP and 2T-DOP were optimized by Gaussian 16 program under M062X/def2SVP level and the wavefunction was checked under BS-DFT to ensure that there is no diradical character in 2T-DPP and 2T-DOP.⁶ We evaluated the weight of excited state through NTO analysis by Multiwfn program.^{7, 8} The simulated vibronic spectra were calculated with FCHT approximation using Gaussian 16 program.⁹

In our calculations, we employed the complete active space configuration interaction (CASCI) and state averaged self-consistent field (SA-CASSCF) methods to compute the low-lying electronic excited states at the DFT optimized geometries. In our study, 2T-DPP undergoes SF to generate ¹TT, while 2T-DOP does not. Because the ¹TT state is a spin-singlet state, we focused on S₁ and ¹TT states of 2T-DPP in the CASSCF calculation. The subsequent evolution from ¹TT state to quintet

and triplet states is beyond the scope of CASSCF calculation at the moment. We chose the six orbitals near highest occupied molecular orbitals (HOMOs) and lowest unoccupied molecular orbitals (LUMOs) into the active space, i.e. CAS (6e, 6o) were applied for the dimer systems (Fig. S24, S25). The electron distribution of these six orbitals is similar to that of HOMOs and LUMOs in each unit (the tetracene unit and the bridge unit). As the charge-transfer states appear high in energy at the SA-CASSCF level of theory, a large number of states (20) are included in the average to calculate the wavefunction.¹⁰ All the CASSCF calculations were performed by the OpenMolcas package with the ANO-L-VDZP basis set.^{11, 12} To characterize the main local feature of the low-lying singlet excited states, a localized molecular orbital set was built from the CASSCF natural orbitals based on the Pipek-Mezey method (Fig. S26 and S27). We then projected the adiabatic excited states onto the space spanned by various local diabatic states using the constructed local molecular orbital set, e.g., local excitation (LE) states, charge transfer (CT) states, triplet pair (TT) states and so on. The calculated and analysis results are shown in Fig. S28, S29. Besides, 10 triplet states were also calculated by the SA-CASSCF method to gain into more insights into the triplets in these two systems. The energies of the lowest two triplet states are shown in Table S7.

The energies of the diabatic states and their electronic couplings are calculated by the equation:

$$\varepsilon_I = \langle \Psi_I | \hat{H} | \Psi_I \rangle = \sum_i |c_{Ii}|^2 E_i \quad (\text{S10})$$

$$V_{IJ} = \langle \Psi_I | \hat{H} | \Psi_J \rangle = \sum_i c_{Ii}^* c_{Ji} E_i \quad (\text{S11})$$

where $|\Psi_I\rangle$ are the constructed local diabatic states, $c_{Ii} = \langle \Phi_I | \Psi_I \rangle$ is the overlap between the adiabatic states $|\Psi_i\rangle$ and local diabatic state $|\Psi_I\rangle$ with E_i being the energy of $|\Psi_i\rangle$. The calculated diabatic electronic Hamiltonians of 2T-DPP and 2T-DOP are shown in Table S4 and S5.

The role of CT states was estimated by calculating the indirect coupling V_{indirect}^{13} :

$$V_{\text{indirect}} = - \frac{2(V_{S_1 S_0, CA} V_{CA, TT} - V_{S_1 S_0, AC} V_{CA, TT})}{\{[E(CT) - E(TT)] + [E(CT) - E(S_1)]\}} \quad (\text{S11})$$

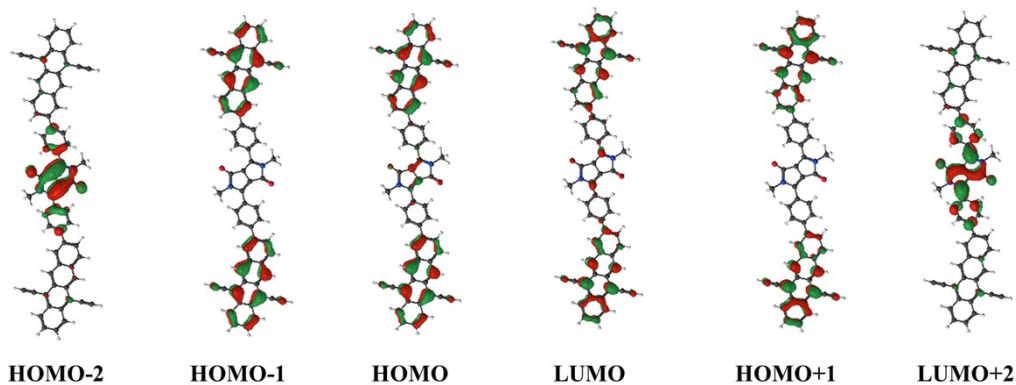


Figure S24. Hartree-Fock molecular orbitals of 2T-DPP.

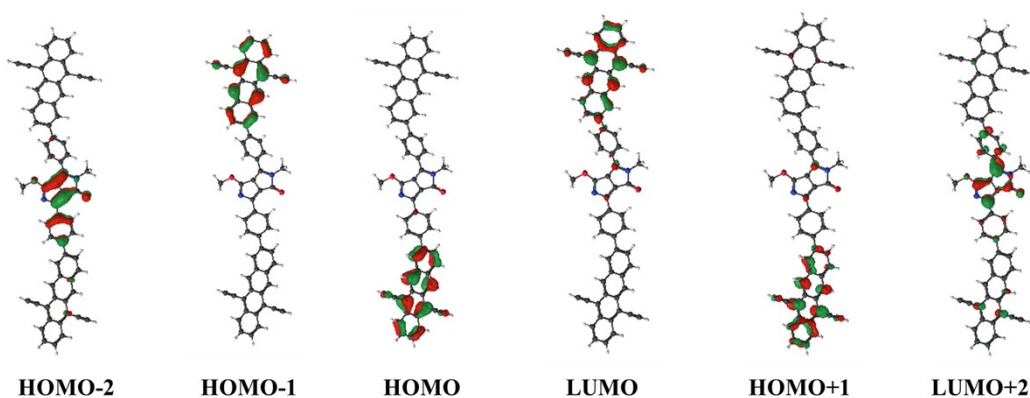


Figure S25. Hartree-Fock molecular orbitals of 2T-DOP.

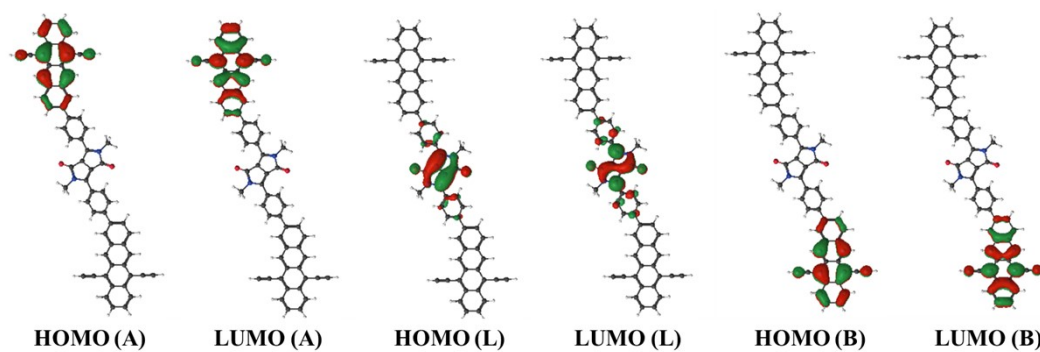


Figure S26. Localized molecular orbitals of 2T-DPP. A and B represent TIPS-TC units. L represents bridge unit.

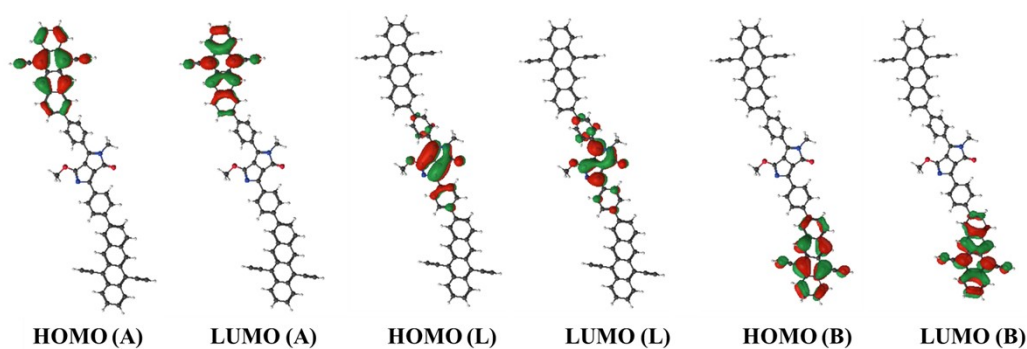


Figure S27. Localized molecular orbitals of 2T-DOP.

	Excitation energy (eV)	Electron density difference	Main components (Weight)
S ₁	3.647		A [†] LB [†] (0.97937)
S ₂	3.886		AL [†] B [†] (-0.69865) A [†] L [†] B (0.67843)
S ₃	3.887		AL [†] B [†] (0.67766) A [†] L [†] B (0.69791)
S ₄	4.170		ALB* (-0.67905) A*LB (0.67943)
S ₅	4.172		ALB* (-0.67927) A*LB (-0.67888)
S ₆	4.904		AL*B (-0.95086)

Figure S28. Excitation energy of the lowest-lying singlet excited states and the plots of the electron density difference between the excited states and the ground state for 2T-DPP. Red: electron. Blue: hole.

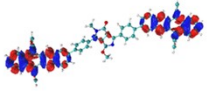
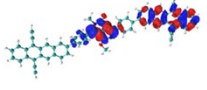
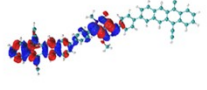
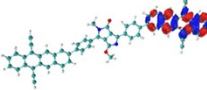
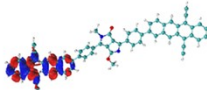
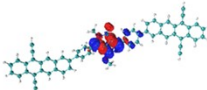
	Excitation energy (eV)	Electron density difference	Main components (Weight)
S_1	3.692		$A^T L B^T$ (0.93752)
S_2	3.737		$A L^T B^T$ (0.94069)
S_3	3.748		$A^T L^T B$ (0.93152)
S_4	4.244		$A L B^*$ (-0.95475)
S_5	4.259		$A^* L B$ (-0.95647)
S_6	4.506		$A L^* B$ (-0.92691)

Figure S29. Excitation energy of the lowest-lying singlet excited states and the plots of the electron density difference between the excited states and the ground state for 2T-DOP. Red: electron. Blue: hole.

Table S4. Electronic Hamiltonian elements of 2T-DPP (unit: eV).

	$A^* L B$	$A L^* B$	$A L B^*$	$A^T L^T B$	$A L^T B^T$	$A^* L B^T$	$A^T L^T B^T$	$A L^+ B^-$	$A^+ L B^-$	$A^+ L B^+$	$A^T L^T B^+$	$A^T L B^T$
$A^* L B$	3.9471	-0.0103	0.0019	0.0994	-0.0002	-0.0006	0.1339	-0.0001	-0.0011	-0.0005	0.0000	-3.2×10^{-7}
$A L^* B$	-0.0103	4.6680	-0.0103	-0.1483	-0.1184	-0.0002	-0.1184	-0.1483	0.0002	-0.0002	0.0002	0.0000
$A L B^*$	0.0019	-0.0103	3.9471	-0.0001	0.1339	0.0011	-0.0002	0.0994	0.0006	0.0000	0.0005	3.2×10^{-7}
$A^T L^T B$	0.0994	-0.1483	-0.0001	6.0887	-0.0020	0.1002	0.0051	0.0002	0.0000	-0.2110	0.0000	0.0000
$A L^T B^T$	-0.0002	-0.1184	0.1339	-0.0020	6.3315	0.1373	-0.0019	0.0051	0.0001	0.0000	-0.1763	0.0000
$A^* L B^T$	-0.0006	-0.0002	0.0011	0.1002	0.1373	6.1870	-0.0001	0.0000	0.0000	-0.0001	-0.0003	-0.0034
$A^+ L B^-$	0.1339	-0.1184	-0.0002	0.0051	-0.0019	-0.0001	6.3314	-0.0020	-0.1373	0.1763	0.0000	0.0000
$A L^+ B^+$	-0.0001	-0.1483	0.0994	0.0002	0.0051	0.0000	-0.0020	6.0887	-0.1002	0.0000	0.2110	0.0000
$A^+ L B^+$	-0.0011	0.0002	0.0006	0.0000	0.0001	0.0000	-0.1373	-0.1002	6.1870	-0.0003	-0.0001	-0.0034
$A^T L^T B^+$	-0.0005	-0.0002	0.0000	-0.2110	0.0000	-0.0001	0.1763	0.0000	-0.0003	3.4229	0.0000	0.0017
$A L^T B^T$	0.0000	0.0002	0.0005	0.0000	-0.1763	-0.0003	0.0000	0.2110	-0.0001	0.0000	3.4229	0.0017
$A^T L B^T$	0.0000	0.0000	0.0000	0.0000	0.0000	-0.0034	0.0000	0.0000	-0.0034	0.0017	0.0017	3.1899

Table S5. Electronic Hamiltonian elements of 2T-DOP (unit: eV).

	A [*] LB	AL [*] B	ALB [*]	A [†] L [†] B	AL [†] B [†]	A [*] LB ⁺	A [†] L [†] B	AL [†] B ⁺	A [*] LB ⁻	A [†] L [†] B	AL [†] B [†]	A [†] LB [†]
A [*] LB	4.0335	-0.0098	0.0016	-0.0920	-0.0003	0.0004	-0.1476	-0.0002	0.0026	0.0007	0.0000	-8.5×10 ⁻⁷
AL [*] B	-0.0098	4.3995	-0.0053	0.1634	-0.1535	0.0006	0.1146	-0.1511	-0.0005	0.0006	0.0001	0.0000
ALB [*]	0.0016	-0.0053	4.0222	0.0001	0.1283	-0.0027	0.0003	0.1465	-0.0004	0.0000	-0.0018	7.6×10 ⁻⁷
A [†] L [†] B	-0.0920	0.1634	0.0001	6.5719	0.0024	0.1458	0.0059	-0.0018	0.0000	-0.2787	0.0001	0.0000
AL [†] B [†]	-0.0003	-0.1535	0.1283	0.0024	5.2734	-0.1516	0.0017	0.0078	0.0000	-0.0001	0.2006	0.0000
A [*] LB ⁺	0.0004	0.0006	-0.0027	0.1458	-0.1516	6.0296	-0.0001	0.0000	0.0000	-0.0004	-0.0005	-0.0032
A [†] L [†] B	-0.1476	0.1146	0.0003	0.0059	0.0017	-0.0001	5.4326	0.0031	-0.1337	0.1480	-0.0001	0.0000
AL [†] B ⁺	-0.0002	-0.1511	0.1465	-0.0018	0.0078	0.0000	0.0031	6.7273	0.0933	0.0001	-0.2677	0.0000
A [*] LB ⁻	0.0026	-0.0005	-0.0004	0.0000	0.0000	0.0000	-0.1337	0.0933	6.4691	-0.0002	-0.0001	-0.0043
A [†] L [†] B	0.0007	0.0006	0.0000	-0.2787	-0.0001	-0.0004	0.1480	0.0001	-0.0002	3.2936	0.0000	0.0029
AL [†] B [†]	0.0000	0.0001	-0.0018	0.0001	0.2006	-0.0005	-0.0001	-0.2677	-0.0001	0.0000	3.2990	0.0021
A [†] LB [†]	0.0000	0.0000	0.0000	0.0000	0.0000	-0.0032	0.0000	0.0000	-0.0043	0.0029	0.0021	3.2272

Table S6. Direct and indirect coupling (eV) of the lowest lying absorbing singlet states A^{*}LB and ALB^{*} to A[†]LB[†] for 2T-DOP and 2T-DPP.

Dimer	State	Direct	Indirect
2T-DPP	A [*] LB	-3.2 × 10 ⁻⁷	6.4 × 10 ⁻⁷
	ALB [*]	-3.2 × 10 ⁻⁷	-1.9 × 10 ⁻⁶
2T-DOP	A [*] LB	-8.5 × 10 ⁻⁷	3.1 × 10 ⁻⁶
	ALB [*]	-7.6 × 10 ⁻⁷	8.6 × 10 ⁻⁶

Table S7. The energy levels of S₁, T₁ and T₂ for 2T-DPP and 2T-DOP.

Compound	Method	S ₁ (eV)	T ₁ (eV)	T ₂ (eV)	E _{S1} - 2 E _{T1} (eV)	E _{T2} - 2 E _{T1} (eV)
2T-DPP	TDDFT	2.47	1.22	2.54	0.03	0.10
	CASCI	3.95	1.82	1.82	0.31	-1.83
2T-DOP	TDDFT	2.44	1.21	2.53	0.02	0.11
	CASCI	4.02	1.84	1.85	0.34	-1.83

The adiabatic excited states of 2T-DPP and 2T-DOP have been studied with TDDFT and CASCI method. The ΔE (E_{S1} - 2 E_{T1}) is positive for both two dimers, suggesting that both systems fulfill the energy requirement for SF.

To estimate whether the bond between phenyl ring and bridge core has a partial

double bond property, the bond lengths are carefully compared in the two dimers. The bond length is 1.464 Å for 2T-DPP and 1.459 Å for 2T-DPP, which are almost identical, suggesting that the specific bond of 2T-DOP does not show stronger double bond property than that of 2T-DPP. Therefore, based on the above analysis, the planar structure of 2T-DOP is mainly attributed to the steric effect.

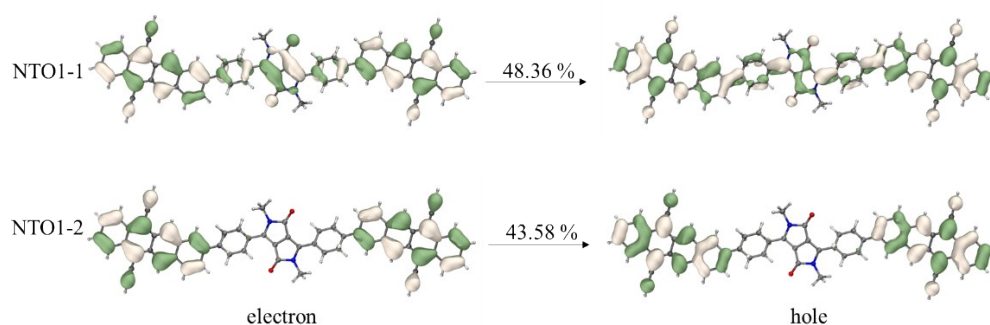


Figure S30. Two main NTOs of S_1 are delocalized in two tetracene chromophores of 2T-DPP at preferential conformation.

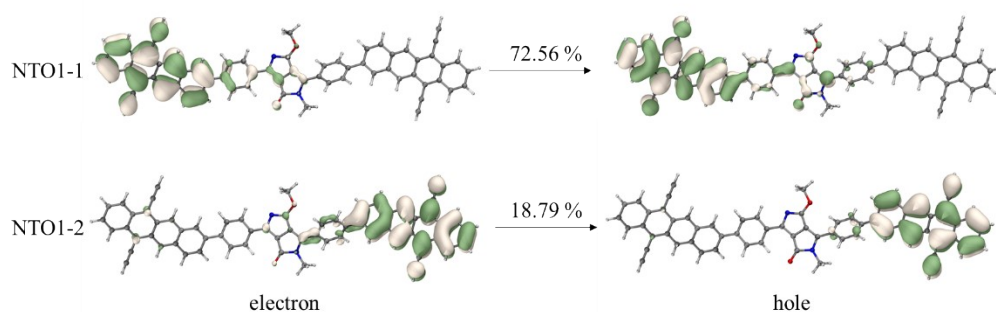


Figure S31. Two main NTOs of S_1 are localized on one side of 2T-DOP at preferential conformation. 2T-DPP has two NTOs with similar weight. One NTO (48.35 %) contains the entire DPP bridge, while the other (43.58 %) does not involve the bridge. For 2T-DOP, both NTOs involve the DOP bridge. The NTO analysis shows the different roles of the DPP and DOP bridges in S_1 transition for the two dimers.

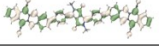
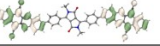
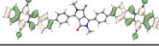
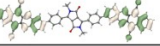

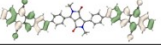
State	NT01-1		NT01-2	
	Orbital transition	weight	Orbital transition	weight
S ₁		0.4836		0.4358
S ₂		0.5021		0.4779
S ₃		0.8865		0.0045

Figure S32. The main NTOs of S₁, S₂ and S₃ for 2T-DPP.

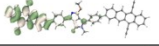
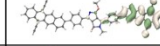
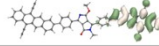
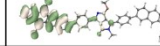
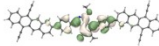
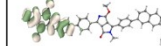
State	NT01-1		NT01-2	
	Orbital transition	weight	Orbital transition	weight
S ₁		0.7256		0.1879
S ₂		0.7889		0.1932
S ₃		0.7657		0.1139

Figure S33. The main NTOs of S₁, S₂ and S₃ for 2T-DOP.

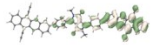
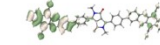
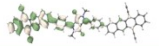
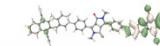
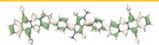
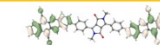
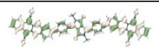
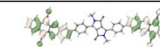
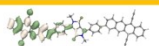
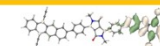
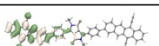
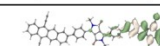
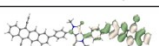
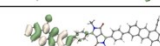
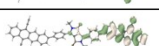
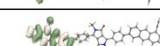
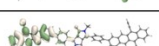
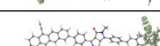
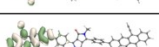

Angle	NT01-1		NT01-2	
	Orbital transition	weight	Orbital transition	weight
-0.62		0.5790		0.2983
9.37		0.5724		0.3127
19.37		0.4983		0.3936
30.44		0.4835		0.4357
39.37		0.5856		0.3438
49.37		0.8731		0.0737
59.37		0.9315		0.0219
69.37		0.9579		0.0054
79.37		0.9502		0
89.37		0.9870		0.0006

Figure S34. The change of the NTOs with different α angles of 2T-DPP. The delocalized NTOs are highlighted by orange line.

Angle	NTO1-1		NTO1-2	
	Orbital transition	weight	Orbital transition	weight
-0.62		0.7255		0.1879
9.37		0.7227		0.1960
19.37		0.7030		0.2303
30.44		0.6551		0.2949
39.37		0.5629		0.3922
49.37		0.6921		0.2883
59.37		0.9210		0.0549
69.37		0.9782		0.0038
79.37		0.9744		0
89.37		0.9916		0

Figure S35. The change of the NTOs with different α angles of 2T-DOP.

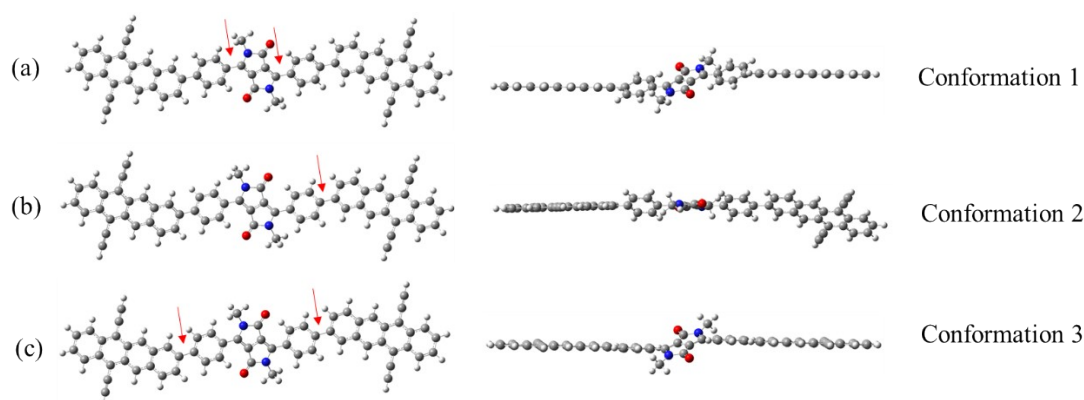


Figure S36. Some specific dihedral angles are set as 0° to break the symmetry of 2T-DPP because the dihedral angle of 90° is inexistent in ambient condition. The dihedral angles with red arrow are 0° . Conformation 1 (a) and 3 (c) have symmetric structure and Conformation 2 (b) has asymmetric structure.

	NTO1-1		NTO1-2	
	Orbital transition	weight	Orbital transition	weight
Conformation 1		0.5908		0.2377
Conformation 2		0.8210		0.0754
Conformation 3		0.5591		0.3509

Figure S37. The NTOs of three conformations in Fig. S36. The symmetric structures (Conformation 1 and 3) have delocalized singlet while that of asymmetric Conformation 2 is localized





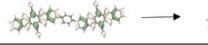
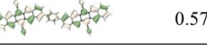
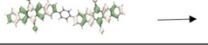
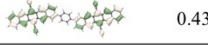

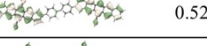

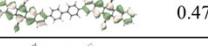





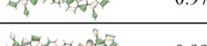


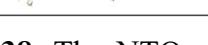
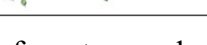


Dimer	NTO1-1		NTO1-2	
	Orbital transition	weight	Orbital transition	weight
P0	 → 	0.6893	 → 	0.3162
P1	 → 	0.5709	 → 	0.4339
P2	 → 	0.5245	 → 	0.4794
T0	 → 	0.9987	 → 	0.0010
T1	 → 	0.9784	 → 	0.0000
T2	 → 	0.9976	 → 	0.0000

Figure S38. The NTOs of pentacene homodimer **P_n** and tetracene homodimer **T_n** ('n' represents the number of benzene). All the heterodimers reported by Sanders *et al.* are delocalized because the S₁ state contains both the GSB of tetracene and pentacene. The difference is the extend of delocalization, which is dependent on the bridge length. Furthermore, the NTOs of homodimers show that all dimers have delocalized exciton, regardless of the bridges and chromophores.

Synthetic information

Compound **1**, DPP¹⁴ and ((8-(4,4,5,5-tetramethyl-1,3,2-dioxaborolan-2-yl)tetracene-5,12-diyl)bis(ethyne-2,1-diyl))bis(triisopropylsilane) (TIPS-Tc-Bpin)¹⁵ were synthesized according to the previously literature procedures.

Compound 2 and Compound 3

In a round bottomed flask were added compound **1** (880 mg, 1.97 mmol), CsCO₃ (1.70 g, 5.21 mmol), 1-Iodohexane (1.24 mL, 8.36 mmol) and MeCN (100 mL). The mixture was heated to reflux and stirred for 12h. After then, the mixture was cooled to room temperature and extracted with DCM and H₂O for 3 times. The organic phase was collected and dried over Na₂SO₄. The crude product was obtained by removing

the solvent then subjected to column chromatography (silica gel, ethyl acetate/petroleum ether = 30/1 to 5/1 v/v). Compound 2 and compound 3 was red solid and orange solid, respectively. Yield: 520 mg, 43 % and 133 mg, 11%.

Compound 2

^1H NMR (400 MHz, CDCl_3): δ 7.70 - 7.65 (m, H), 3.74 - 3.70 (m, 4H), 1.56 (s, 4H), 1.26 - 1.20 (m, 12H), 0.86 - 0.80 (m, 6H).

^{13}C NMR (150 MHz, CDCl_3): δ 162.43 147.43 132.25 130.09 126.96 125.81 109.93 41.89 31.18 29.39 26.35 22.45 13.93

MALDI-MS for $\text{C}_{30}\text{H}_{34}\text{Br}_2\text{N}_2\text{O}_2$. m/z calculated: 614.42; found: 613.996

Compound 3

^1H NMR (400 MHz, CDCl_3): δ 8.32 (d, J = 16.0 Hz, 2H), 7.62 - 7.60 (m, 2H), 7.58 - 7.48 (m, 4H), 4.45 (s, 2H), 3.64 (t, J = 8 Hz, 2H), 1.69 - 1.64 (m, 2H), 1.51 (s, 2H), 1.32 - 1.15 (m, 12H), 0.86 - 0.75 (m, 6H).

^{13}C NMR (150 MHz, CDCl_3): δ 161.54 131.17 130.78 129.37 129.30 126.04 125.27 124.63 40.93 30.34 30.17 27.74 25.34 24.55 21.57 21.44

MALDI-MS for $\text{C}_{30}\text{H}_{34}\text{Br}_2\text{N}_2\text{O}_2$. m/z calculated: 614.42; found: 614.003

Compound 2T-DPP

In a round bottomed flask were added TIPS-Tc-Bpin (466 mg, 0.65 mmol), Compound 2 (184 mg, 0.30 mmol), $\text{Pd}(\text{dppf})\text{Cl}_2$ (10 mg, 0.25 mmol), K_2CO_3 (450 mg, 3.25 mmol) and $\text{THF}/\text{H}_2\text{O}$ = 54 mL/6 mL. The reaction mixture was bubbled by nitrogen for 30 min then heated at 65 °C with stirring for 12 h. The mixture was cooled to room temperature and extracted with DCM and H_2O for 3 times. The

organic phase was collected and dried over Na₂SO₄. The crude product was obtained by removing the solvent then subjected to column chromatography (silica gel, DCM/petroleum ether = 1/5 v/v). Compound 2T-DPP was red solid. Yield: 121 mg, 25 %.

¹H NMR (400 MHz, CDCl₃): δ 9.36 (d, J = 10.0 Hz, 4H), 8.67 - 8.63 (m, 4H), 8.29 (s, 2H), 8.14 (d, J = 4.0 Hz, 2H), 8.07 - 7.99 (m, 8H), 7.88 (d, J = 4.0 Hz, 2H), 7.58 - 7.56 (m, 4H), 3.90 (d, J = 8.0 Hz, 4H), 1.74 (s, 4H), 1.63 (s, 4H), 1.42 - 1.26 (m, 92H), 0.87 (d, J = 4.0 Hz, 6H).

¹³C NMR (150 MHz, CDCl₃): δ 162.92 148.06 163.46 137.08 132.86 132.77 132.15 131.44 130.67 129.63 129.45 127.67 127.47 127.44 127.01 126.87 126.50 126.28 125.47 118.76 110.15 106.22 106.03 103.85 31.29 29.56 23.50 22.54 19.01 18.98 14.01 11.64

MALDI-MS for C₁₁₀H₁₃₆N₂O₂Si₄. *m/z* calculated: 1630.65; found: 1630.748

Compound 2T-DOP

In a round bottomed flask were added TIPS-Tc-Bpin (466 mg, 0.65 mmol), Compound 3 (184 mg, 0.30 mmol), Pd(dppf)Cl₂ (10 mg, 0.25 mmol), K₂CO₃ (450 mg, 3.25 mmol) and THF/H₂O = 54 mL/6 mL. The reaction mixture was bubbled by nitrogen for 30 min then heated at 65 °C with stirring for 12 h. The mixture was cooled to room temperature and extracted with DCM and H₂O for 3 times. The organic phase was collected and dried over Na₂SO₄. The crude product was obtained by removing the solvent then subjected to column chromatography (silica gel, DCM/petroleum ether = 1/5 v/v). Compound 2T-DOP was red solid. Yield: 135 mg,

28 %.

^1H NMR (400 MHz, CDCl_3): δ 9.40 - 9.33 (m, 4H), 8.75 (d, J = 8.0 Hz, 8H), 8.66 - 8.63 (m, 4H), 8.29 (s, 2H), 8.17 - 8.11 (m, 2H), 7.99 - 7.91 (m, 6H), 7.86 - 7.80 (m, 2H), 7.75 - 7.55 (m, 4H), 4.62 (s, 2H), 3.88 (d, J = 8.0 Hz, 2H), 1.84 (d, J = 8.0 Hz, 2H), 1.74 (s, 2H), 1.39 - 1.32 (m, 96H), 0.96 - 0.86 (m, 6H).

^{13}C NMR (150 MHz, CDCl_3): δ 132.75 131.49 131.42 130.77 130.63 129.84 129.75 127.45 127.34 126.97 126.77 126.37 118.70 31.40 31.34 31.28 29.75 28.88 26.50 26.48 25.63 22.65 22.62 22.54 22.51 19.00 18.98 14.01 13.99 13.98 11.62

MALDI-MS for $\text{C}_{110}\text{H}_{136}\text{N}_2\text{O}_2\text{Si}_4$. m/z calculated: 1630.65; found: 1630.754

^1H and ^{13}C NMR spectra

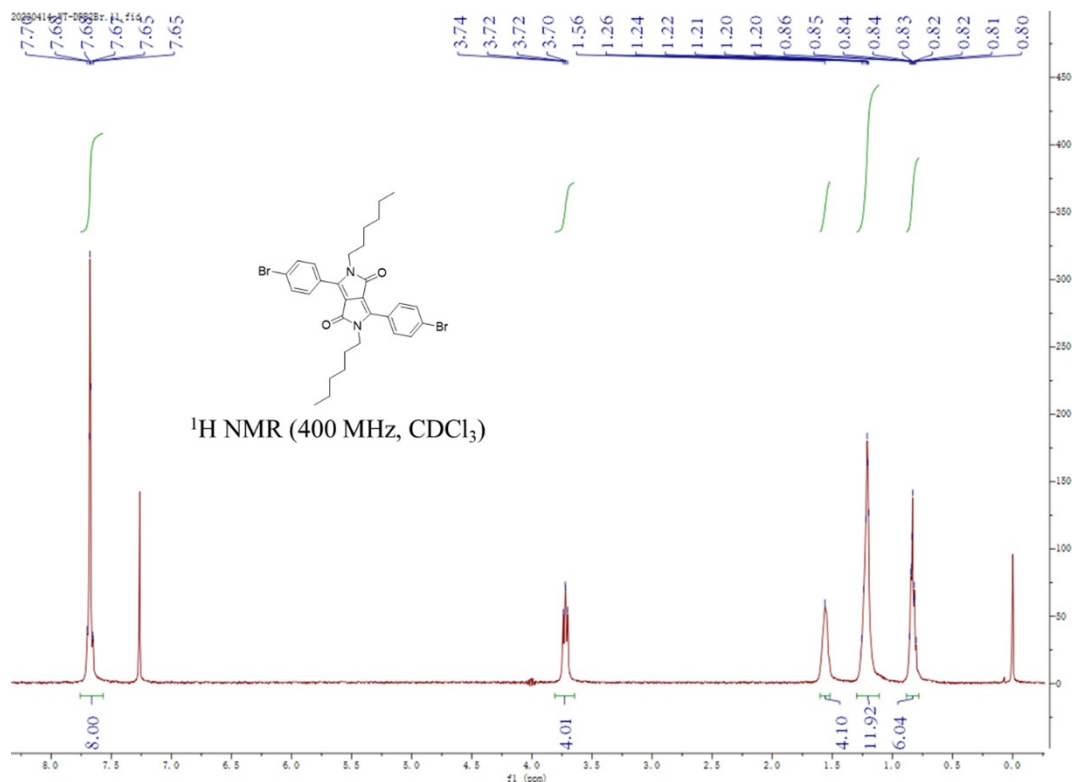


Figure S39. ^1H NMR spectrum of Compound 2 in CDCl_3 .

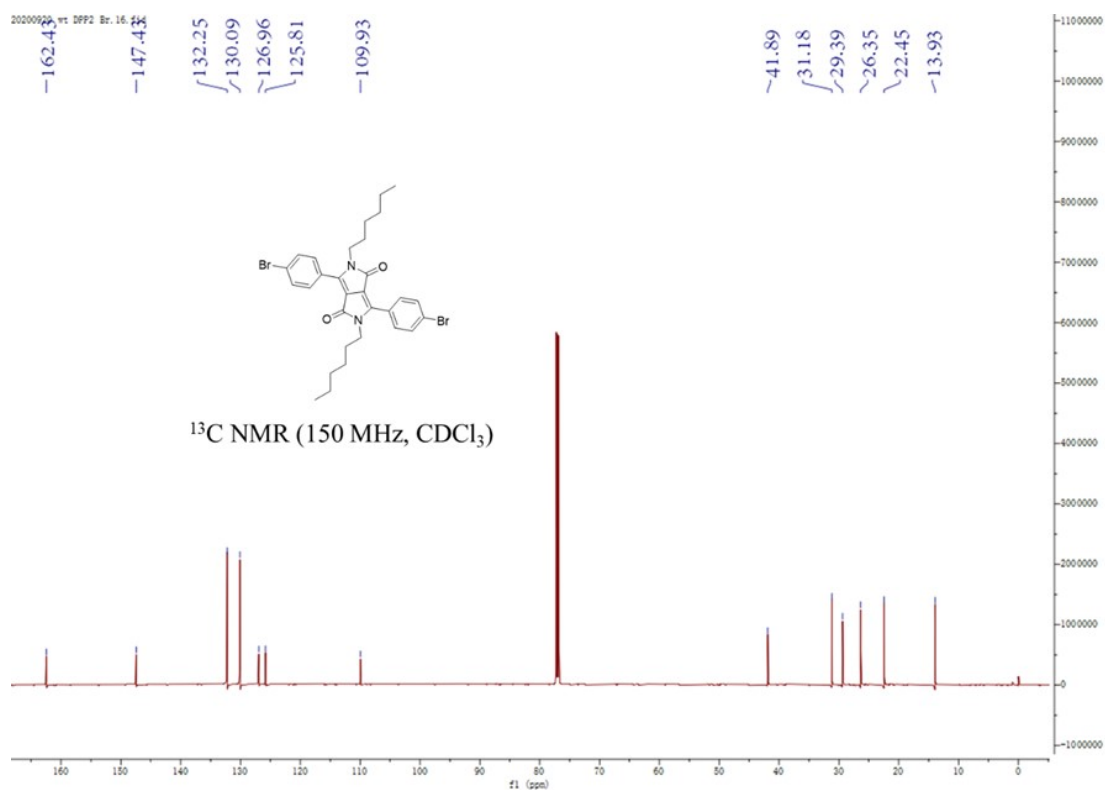


Figure S40. ^{13}C NMR spectrum of Compound 2 in CDCl_3 .

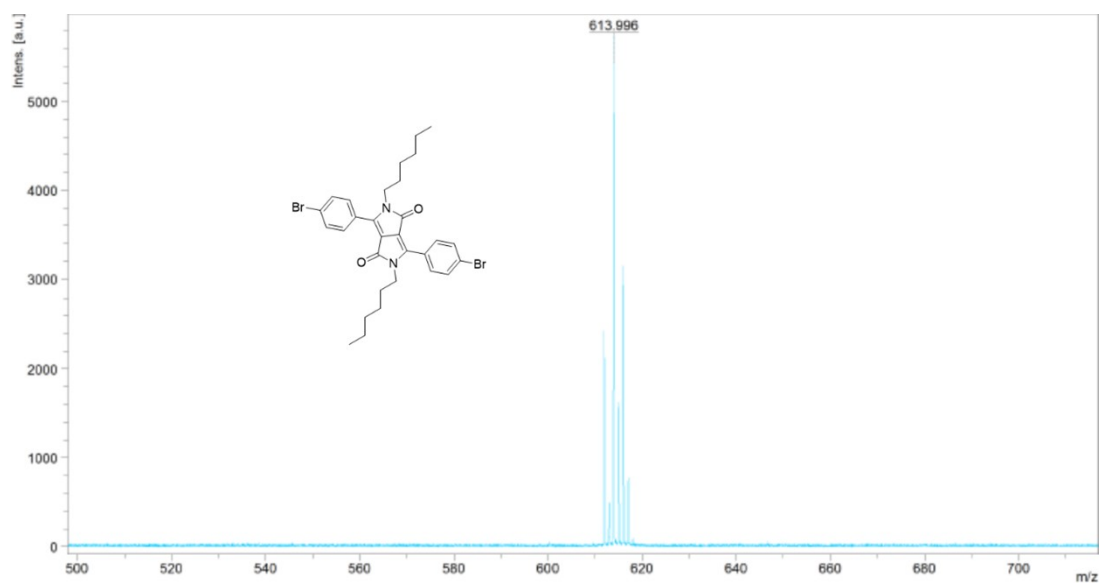


Figure S41. MALDI-MS of Compound 2.

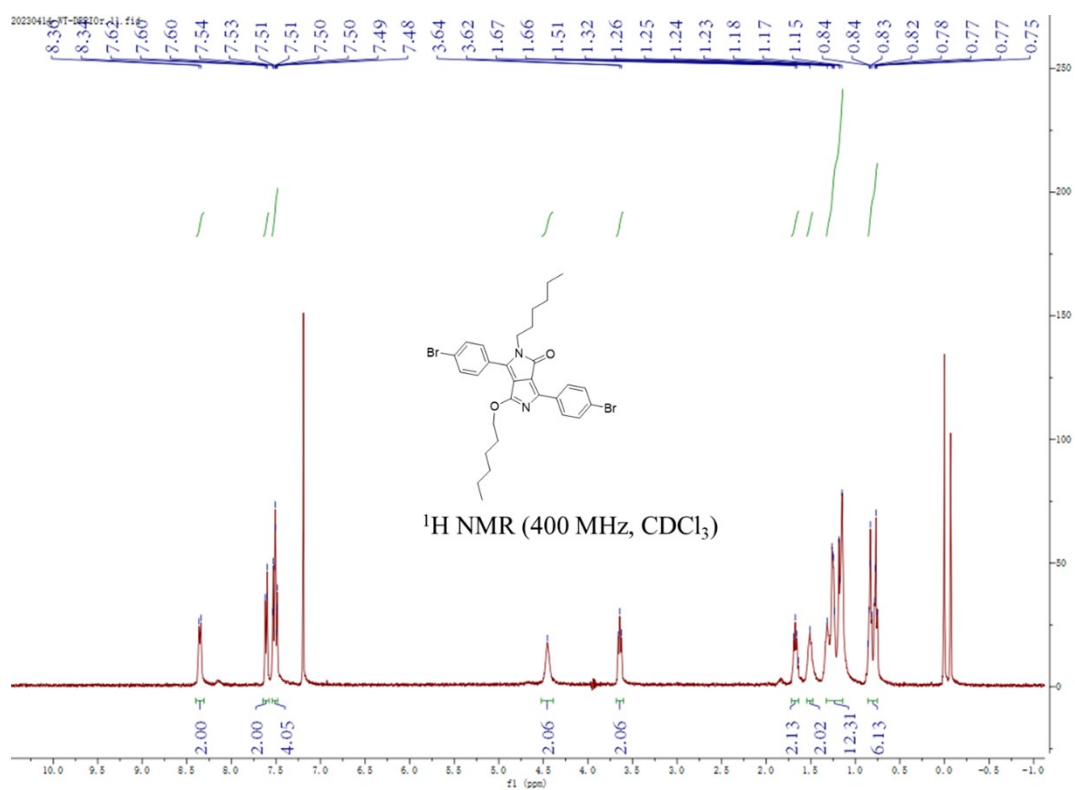


Figure S42. ¹H NMR spectrum of Compound 3 in CDCl₃.

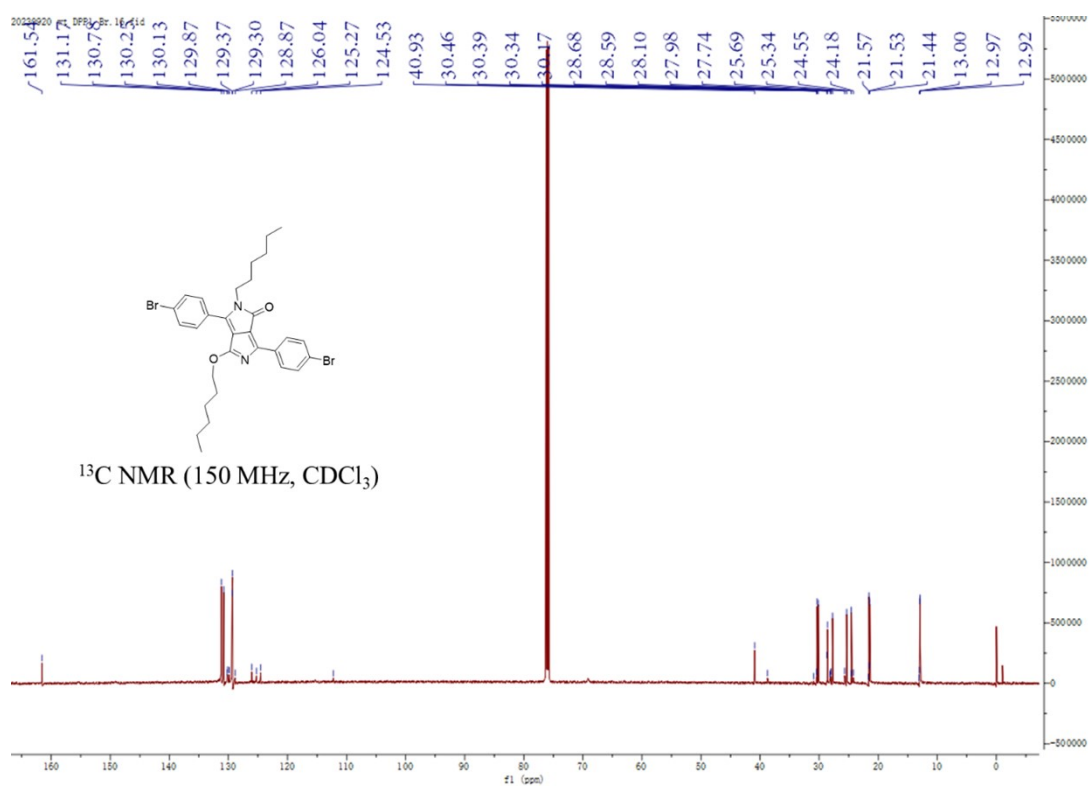


Figure S43. ¹³C NMR spectrum of Compound 3 in CDCl₃.

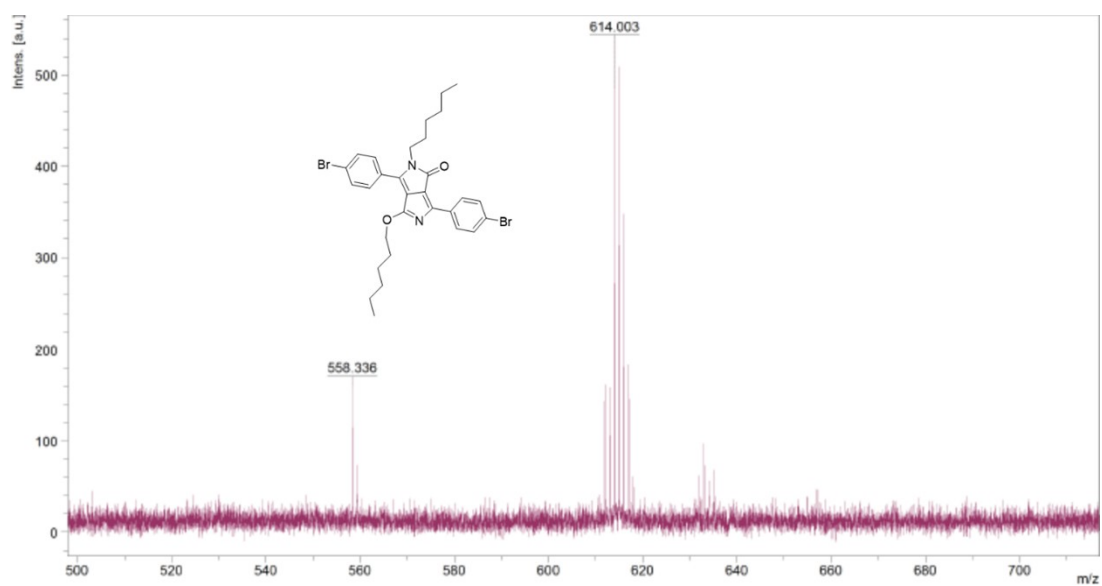


Figure S44. MALDI-MS of Compound 3.

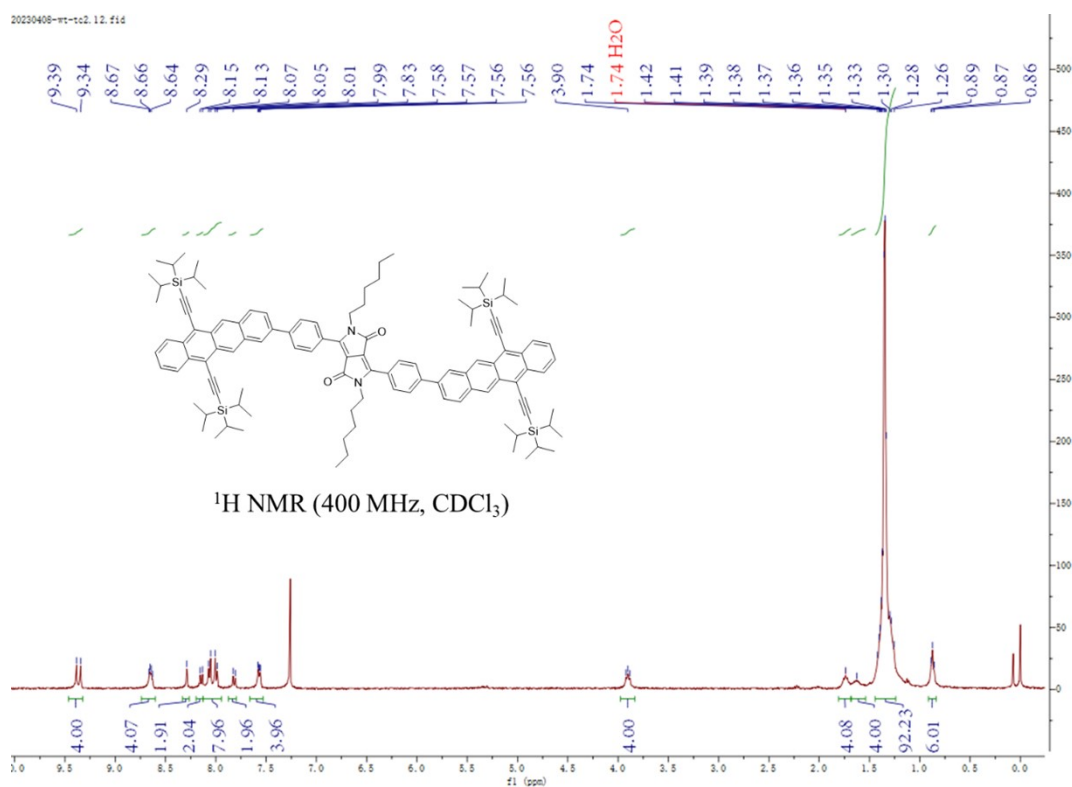


Figure S45. ¹H NMR spectrum of compound 2T-DPP in CDCl₃.

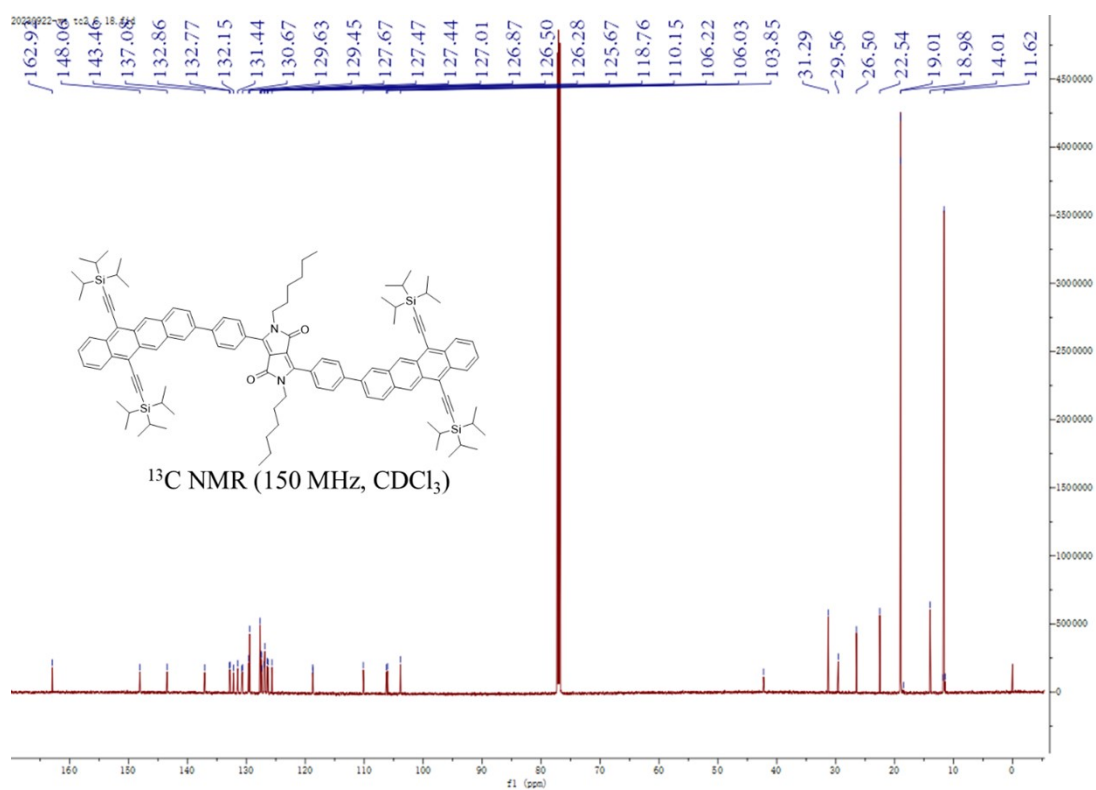


Figure S46. ¹³C NMR spectrum of compound 2T-DPP in CDCl₃.

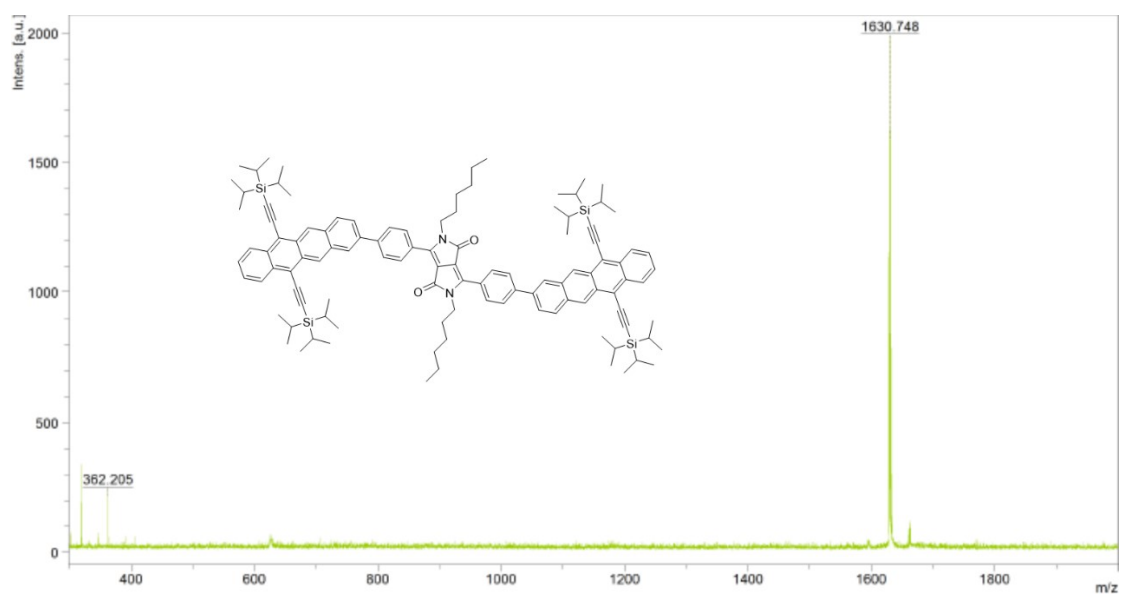


Figure S47. MALDI-MS of 2T-DPP.

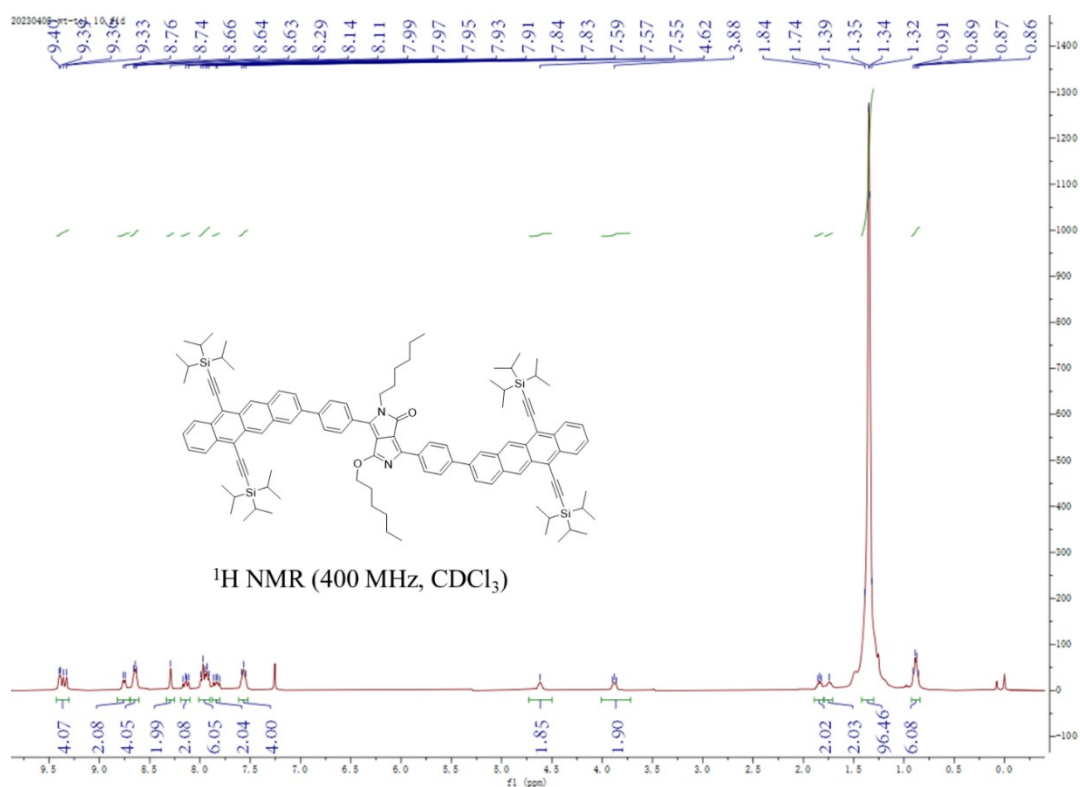


Figure S48. ¹H NMR spectrum of compound 2T-DOP in CDCl₃.

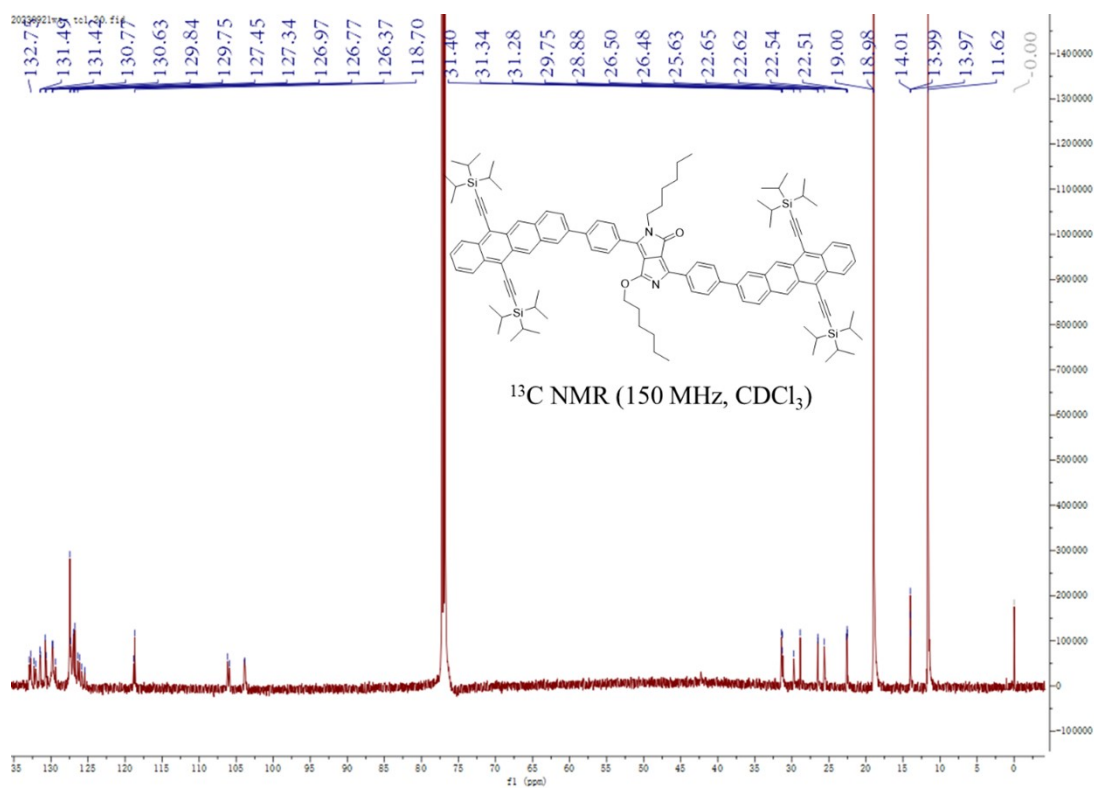


Figure S49. ¹³C NMR spectrum of compound 2T-DOP in CDCl₃.

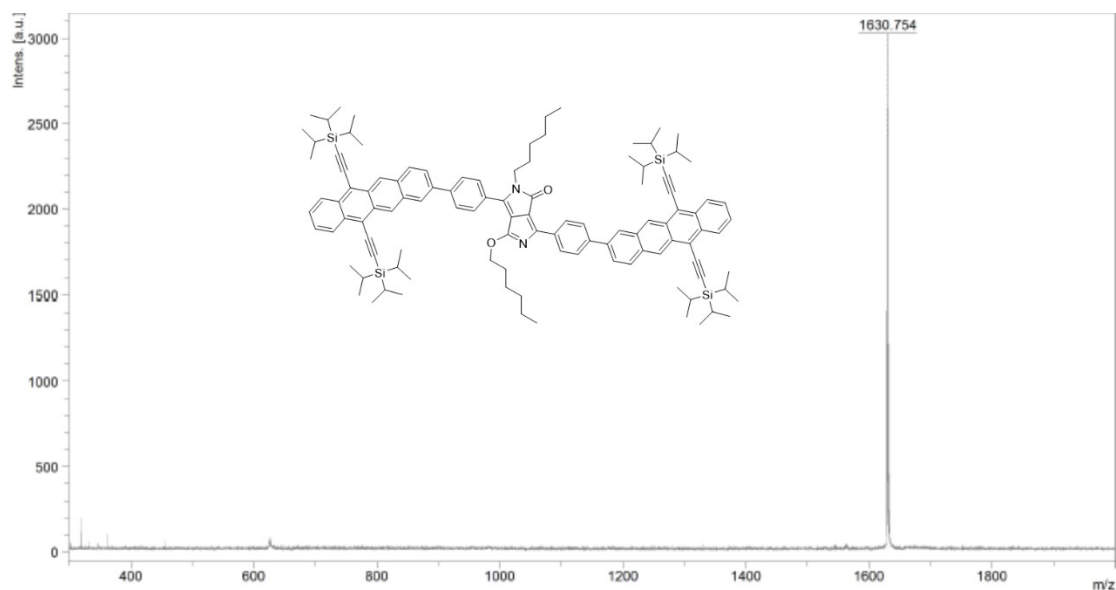


Figure S50. MALDI-MS of 2T-DOP.

Cartesian coordinates

DPP-Br Cartesian Coordinates:

O	-1.2035	2.69371	0.18658
C	-0.44152	1.75116	0.124
N	0.9738	1.89481	0.15444
C	1.61109	0.66676	0.07076
C	-0.64255	0.31152	0.00611
C	1.5604	3.19554	0.40891
H	2.42181	3.09976	1.0805
H	0.78976	3.80985	0.88851
C	3.06606	0.48655	0.05577
C	3.94153	1.43797	-0.49191
C	5.31341	1.20767	-0.52056
C	4.96593	-0.94954	0.53882
H	5.37147	-1.8796	0.93653
H	5.98688	1.94671	-0.95378
H	3.55957	2.35761	-0.93167
C	3.59627	-0.71415	0.55755
H	2.92605	-1.47557	0.95711
C	-1.61109	-0.66674	-0.07081
N	-0.9738	-1.8948	-0.15448
C	0.64256	-0.3115	-0.00618
C	0.44153	-1.75114	-0.1241
O	1.2035	-2.69369	-0.18664

C	-1.5604	-3.19553	-0.4089
H	-2.42184	-3.09976	-1.08046
H	-0.78979	-3.80984	-0.88851
C	-3.06606	-0.48653	-0.0558
C	-3.94151	-1.43796	0.4919
C	-5.31339	-1.20767	0.52057
C	-4.96595	0.94954	-0.53881
H	-5.3715	1.87959	-0.93652
H	-5.98685	-1.94672	0.95381
H	-3.55953	-2.3576	0.93165
C	-3.59629	0.71415	-0.55756
H	-2.92608	1.47558	-0.95714
H	-1.87034	-3.69725	0.51882
H	1.87037	3.69728	-0.51879
C	-5.81591	-0.01804	-0.00355
C	5.81591	0.01803	0.00358
Br	-7.68118	0.29367	0.02077
Br	7.68118	-0.29369	-0.02071

DOP-Br Cartesian Coordinates:

O	1.17909	-2.93397	0.22547
C	0.46629	-1.95581	0.18418
N	-0.96648	-2.05717	0.14643
C	-1.54876	-0.81364	0.13204
C	0.72216	-0.52205	0.18236
C	-1.60795	-3.34962	0.28917
H	-2.50959	-3.25929	0.90639
H	-0.89146	-4.01603	0.78295
C	-2.99338	-0.58083	0.06584
C	-3.85796	-1.43031	-0.64249
C	-5.2188	-1.15274	-0.71483
C	-4.87763	0.84101	0.63321
H	-5.28327	1.72217	1.1298
H	-5.88617	-1.80795	-1.27395
H	-3.47115	-2.29982	-1.17227
C	-3.51733	0.56215	0.69129
H	-2.85031	1.23549	1.23025
C	1.68751	0.4752	0.09373
N	1.0911	1.72582	0.0458
C	-0.54096	0.13866	0.17402
C	-0.21135	1.53761	0.08345
C	3.14167	0.34725	0.04017

C	3.94586	1.4913	-0.08059
C	5.33106	1.38218	-0.13537
C	5.13669	-1.03511	0.05372
H	5.61098	-2.01505	0.10641
H	5.95523	2.27082	-0.22965
H	3.46587	2.46838	-0.13145
C	3.75208	-0.91634	0.10828
H	3.13447	-1.81216	0.20395
H	-1.86965	-3.78712	-0.68445
O	-1.10056	2.5128	0.06393
C	-0.59519	3.83996	-0.03308
H	0.05095	4.06417	0.82557
H	-0.01422	3.95915	-0.95683
H	-1.46829	4.49853	-0.04056
C	5.91461	0.11687	-0.06841
C	-5.71884	-0.02278	-0.0684
Br	-7.57026	0.34778	-0.14912
Br	7.80075	-0.04064	-0.14479

2T-DPP Cartesian Coordinates:

O	-1.00576	-2.76565	-0.0563
C	-0.31341	-1.76958	-0.03331
N	1.10977	-1.80989	-0.03257
C	1.65578	-0.5348	-0.00974
C	-0.6177	-0.34505	-0.00399
C	1.79437	-3.07505	-0.2064
H	2.66217	-2.95086	-0.86504
H	1.08136	-3.76859	-0.66702
C	3.09196	-0.24883	0.02095
C	4.02681	-1.10167	0.6316
C	5.37326	-0.76185	0.66854
C	5.83617	0.43268	0.09473
C	4.89482	1.29091	-0.49608
H	5.22279	2.22323	-0.95775
H	6.07423	-1.42363	1.17909
H	3.70312	-2.01917	1.12018
C	3.5466	0.96079	-0.53073
H	2.83168	1.64591	-0.98691
C	-1.65691	0.55726	0.02363
N	-1.11647	1.83207	0.06323
C	0.61717	0.37331	-0.00793
C	0.30532	1.79812	0.04465

O	0.991	2.79995	0.06672
C	-1.81914	3.0894	0.21371
H	-2.69687	2.9571	0.85763
H	-1.12515	3.7979	0.68048
C	-3.09471	0.27348	0.04687
C	-4.02177	1.04675	-0.67023
C	-5.36735	0.70158	-0.68039
C	-5.83166	-0.42214	0.02161
C	-4.89552	-1.20514	0.71559
H	-5.22729	-2.08106	1.27472
H	-6.06584	1.29665	-1.2703
H	-3.68818	1.90522	-1.25307
C	-3.54765	-0.86919	0.72434
H	-2.83217	-1.49515	1.25873
H	-2.13536	3.5033	-0.75459
H	2.11945	-3.50417	0.75213
C	-7.2717	-0.77726	0.02433
C	-7.66792	-2.16486	0.06473
C	-8.24185	0.19038	-0.00727
C	-8.97978	-2.52601	0.06675
H	-6.89588	-2.93554	0.06698
C	-9.6366	-0.14441	-0.00274
H	-7.96919	1.24779	-0.01188
C	-10.01917	-1.53392	0.03493
H	-9.26464	-3.57954	0.08345
C	-10.62497	0.83406	-0.03034
C	-11.36602	-1.87328	0.03694
C	-11.99431	0.50103	-0.02876
H	-10.33672	1.8861	-0.0563
C	-12.37549	-0.88931	0.00511
H	-11.65327	-2.92553	0.06365
C	-13.009	1.50371	-0.0611
C	-13.75883	-1.23594	0.00573
C	-14.36964	1.15031	-0.06091
C	-14.7501	-0.2395	-0.02705
C	7.27743	0.78109	0.1127
C	7.67984	2.16428	0.20816
C	8.24367	-0.18778	0.03173
C	8.9931	2.51985	0.21957
H	6.91183	2.93364	0.29816
C	9.63966	0.14156	0.03718
H	7.96661	-1.23938	-0.06707
C	10.02816	1.52674	0.131
H	9.28263	3.56881	0.30469

C	10.62375	-0.83769	-0.05162
C	11.37623	1.86099	0.13442
C	11.99435	-0.50986	-0.04902
H	10.33104	-1.88632	-0.12427
C	12.38141	0.87603	0.04576
H	11.66785	2.90993	0.20634
C	13.00466	-1.51352	-0.1379
C	13.76598	1.21756	0.04658
C	14.36664	-1.16527	-0.13554
C	14.75293	0.22022	-0.04275
C	-15.40586	2.14422	-0.0942
H	-15.11488	3.19455	-0.11977
C	-16.14801	-0.56823	-0.02817
H	-16.43212	-1.62043	-0.00258
C	15.39852	-2.16027	-0.22418
H	15.10315	-3.20737	-0.29397
C	16.152	0.54387	-0.04405
H	16.44051	1.59287	0.0258
C	-17.09931	0.40792	-0.06063
H	-18.15655	0.13992	-0.06113
C	-16.72179	1.78748	-0.09417
H	-17.49545	2.55584	-0.11994
C	16.71578	-1.80849	-0.2216
H	17.48612	-2.57762	-0.28974
C	17.09906	-0.43315	-0.13016
H	18.15728	-0.16906	-0.12969
C	-14.13615	-2.61905	0.03987
C	-14.44965	-3.78977	0.06889
H	-14.72961	-4.82809	0.09451
C	-12.62918	2.88602	-0.09475
C	-12.30224	4.05311	-0.12316
H	-12.01417	5.08923	-0.14817
C	12.61905	-2.89154	-0.23023
C	12.28732	-4.05504	-0.30757
H	11.99501	-5.08798	-0.37623
C	14.14911	2.59637	0.13931
C	14.46746	3.76351	0.21745
H	14.75161	4.7987	0.28659

2T-DOP Cartesian Coordinates:

O	-0.9203	-3.21148	0.08326
C	-0.28633	-2.19727	-0.11009
N	1.14569	-2.16147	-0.00056

C	1.63367	-0.91098	-0.29389
C	-0.64887	-0.83976	-0.4913
C	1.88736	-3.38723	0.22027
H	2.80522	-3.38871	-0.37942
H	1.24381	-4.21744	-0.09239
C	3.05057	-0.54819	-0.25213
C	3.95053	-1.11939	0.66312
C	5.27783	-0.71236	0.69044
C	5.75435	0.26593	-0.1971
C	4.84654	0.8439	-1.09926
H	5.19039	1.59726	-1.80916
H	5.95096	-1.14129	1.43378
H	3.60806	-1.85503	1.3895
C	3.51605	0.44822	-1.12582
H	2.82581	0.90487	-1.83549
C	-1.69184	0.05822	-0.69977
N	-1.1933	1.32607	-0.95895
C	0.55868	-0.09235	-0.61399
C	0.11959	1.24829	-0.90147
C	-3.13178	-0.17747	-0.66814
C	-4.02822	0.88133	-0.88727
C	-5.39865	0.66115	-0.86096
C	-5.92063	-0.61988	-0.61356
C	-5.01814	-1.67577	-0.40115
H	-5.39583	-2.67762	-0.19095
H	-6.07903	1.49075	-1.05999
H	-3.62636	1.87435	-1.08792
C	-3.64561	-1.46232	-0.4245
H	-2.95917	-2.29329	-0.24841
H	2.13993	-3.52844	1.28055
C	-7.38441	-0.85273	-0.57308
C	-7.92303	-2.11346	-1.02693
C	-8.24652	0.10616	-0.10712
C	-9.26042	-2.36265	-1.00445
H	-7.24016	-2.86851	-1.41878
C	-9.66298	-0.11424	-0.06182
H	-7.86491	1.05853	0.26678
C	-10.18723	-1.37691	-0.51985
H	-9.65324	-3.31567	-1.36355
C	-10.54039	0.85398	0.4158
C	-11.55687	-1.60413	-0.48272
C	-11.93172	0.63415	0.45831
H	-10.14496	1.80897	0.76537
C	-12.4547	-0.62801	-0.00358

H	-11.95069	-2.56008	-0.83148
C	-12.83264	1.62776	0.94526
C	-13.86133	-0.85919	0.03519
C	-14.21761	1.38901	0.97848
C	-14.73971	0.1274	0.51676
C	7.17847	0.67822	-0.18374
C	7.53377	2.0443	-0.48622
C	8.17287	-0.22021	0.10349
C	8.83148	2.45338	-0.48669
H	6.74044	2.76424	-0.69208
C	9.55406	0.166	0.10778
H	7.9332	-1.26535	0.31025
C	9.89631	1.5337	-0.19335
H	9.08491	3.49266	-0.70343
C	10.56732	-0.74448	0.38884
C	11.22992	1.92182	-0.19136
C	11.92356	-0.36203	0.39159
H	10.3094	-1.78045	0.61408
C	12.26457	1.00738	0.09483
H	11.48641	2.95796	-0.41743
C	12.96364	-1.29519	0.68011
C	13.63462	1.40339	0.09613
C	14.31073	-0.8937	0.67797
C	14.65132	0.47527	0.38181
C	-15.14056	2.37634	1.46438
H	-14.74254	3.32954	1.81303
C	-16.15907	-0.08587	0.56309
H	-16.55044	-1.04127	0.21299
C	15.37203	-1.81759	0.96557
H	15.11126	-2.85225	1.18911
C	16.0365	0.85411	0.38751
H	16.29049	1.89023	0.16289
C	-16.99974	0.87958	1.0323
H	-18.07523	0.70037	1.06026
C	-16.48162	2.13187	1.49069
H	-17.1679	2.89344	1.86305
C	16.67455	-1.41491	0.96022
H	17.46778	-2.13017	1.18102
C	17.01254	-0.05616	0.66619
H	18.05962	0.2491	0.66604
C	-14.37954	-2.11516	-0.42377
C	-14.81283	-3.17871	-0.81213
H	-15.19889	-4.12176	-1.15676
C	-12.31213	2.88268	1.40397

C	-11.86553	3.9417	1.78976
H	-11.4708	4.88167	2.13296
C	12.62356	-2.65682	0.97405
C	12.33028	-3.80687	1.22126
H	12.07271	-4.82802	1.44059
C	13.97203	2.76574	-0.19818
C	14.25186	3.91874	-0.44709
H	14.50162	4.94159	-0.66754
O	0.92855	2.27275	-1.10357
C	0.31544	3.52977	-1.36525
H	-0.29866	3.4721	-2.27334
H	-0.32354	3.82467	-0.52265
H	1.13177	4.24563	-1.49725

3. Reference

1. L. Wang, T.-S. Zhang, L. Fu, S. Xie, Y. Wu, G. Cui, W.-H. Fang, J. Yao and H. Fu, *J. Am. Chem. Soc.*, 2021, **143**, 5691-5697.
2. L. Wang, L. Lin, J. Yang, Y. Wu, H. Wang, J. Zhu, J. Yao and H. Fu, *J. Am. Chem. Soc.*, 2020, **142**, 10235-10239.
3. J. Snellenburg, S. Liptonok, R. Seger, K. Mullen and I. Van Stokkum, *J. STAT. SOFTW*, 2012, **49**, 1-22.
4. L. R. K. Snyder, J. J.; Glajch, J. L., in *Practical HPLC Method Development*, John Wiley & Sons, Inc., 1997, pp. 721-728.
5. S. Nakamura, H. Sakai, H. Nagashima, M. Fuki, K. Onishi, R. Khan, Y. Kobori, N. V. Tkachenko and T. Hasobe, *J. Phys. Chem. C*, 2021, **125**, 18287-18296.
6. M. J. Frisch, G. W. Trucks, H. B. Schlegel, G. E. Scuseria, M. A. Robb, J. R. Cheeseman, G. Scalmani, V. Barone, G. A. Petersson, H. Nakatsuji, X. Li, M. Caricato, A. V. Marenich, J. Bloino, B. G. Janesko, R. Gomperts, B. Mennucci, H. P. Hratchian, J. V. Ortiz, A. F. Izmaylov, J. L. Sonnenberg, Williams, F. Ding, F. Lipparini, F. Egidi, J. Goings, B. Peng, A. Petrone, T. Henderson, D. Ranasinghe, V. G. Zakrzewski, J. Gao, N. Rega, G. Zheng, W. Liang, M. Hada, M. Ehara, K. Toyota, R. Fukuda, J. Hasegawa, M. Ishida, T. Nakajima, Y. Honda, O. Kitao, H. Nakai, T. Vreven, K. Throssell, J. A. Montgomery Jr., J. E. Peralta, F. Ogliaro, M. J. Bearpark, J. J. Heyd, E. N. Brothers, K. N. Kudin, V. N. Staroverov, T. A. Keith, R. Kobayashi, J. Normand, K. Raghavachari, A. P. Rendell, J. C. Burant, S. S. Iyengar, J. Tomasi, M. Cossi, J. M. Millam, M. Klene, C. Adamo, R. Cammi, J. W. Ochterski, R. L. Martin, K. Morokuma, O. Farkas, J. B. Foresman and D. J. Fox, *Journal*, 2016.
7. T. Lu and F. Chen, *J. Comput. Chem*, 2012, **33**, 580-592.
8. W. Humphrey, A. Dalke and K. Schulten, *J. Mol. Graph*, 1996, **14**, 33-38.

9. T. Teramoto, J. Liu, J. Du and T. Kobayashi, *Phys. Chem. Chem. Phys.*, 2022, **24**, 27783-27792.
10. B. S. Basel, J. Zirzmeier, C. Hetzer, B. T. Phelan, M. D. Krzyaniak, S. R. Reddy, P. B. Coto, N. E. Horwitz, R. M. Young, F. J. White, F. Hampel, T. Clark, M. Thoss, R. R. Tykwinski, M. R. Wasielewski and D. M. Guldi, *Nat. Commun.*, 2017, **8**, 15171.
11. F. Aquilante, J. Autschbach, R. K. Carlson, L. F. Chibotaru, M. G. Delcey, L. De Vico, I. Fdez. Galván, N. Ferré, L. M. Frutos, L. Gagliardi, M. Garavelli, A. Giussani, C. E. Hoyer, G. Li Manni, H. Lischka, D. Ma, P. Å. Malmqvist, T. Müller, A. Nenov, M. Olivucci, T. B. Pedersen, D. Peng, F. Plasser, B. Pritchard, M. Reiher, I. Rivalta, I. Schapiro, J. Segarra-Martí, M. Stenrup, D. G. Truhlar, L. Ungur, A. Valentini, S. Vancoillie, V. Veryazov, V. P. Vysotskiy, O. Weingart, F. Zapata and R. Lindh, *J. Comput. Chem.*, 2016, **37**, 506-541.
12. Z. Wang, H. Liu, X. Xie, C. Zhang, R. Wang, L. Chen, Y. Xu, H. Ma, W. Fang, Y. Yao, H. Sang, X. Wang, X. Li and M. Xiao, *Nat. Chem.*, 2021, **13**, 559-567.
13. J. Zirzmeier, R. Casillas, S. R. Reddy, P. B. Coto, D. Lehnher, E. T. Chernick, I. Papadopoulos, M. Thoss, R. R. Tykwinski and D. M. Guldi, *Nanoscale*, 2016, **8**, 10113-10123.
14. P. E. Hartnett, E. A. Margulies, C. M. Mauck, S. A. Miller, Y. Wu, Y.-L. Wu, T. J. Marks and M. R. Wasielewski, *J. Phys. Chem. B*, 2016, **120**, 1357-1366.
15. A. T. Gilligan, E. G. Miller, T. Sammakia and N. H. Damrauer, *J. Am. Chem. Soc.*, 2019, **141**, 5961-5971.